

## Tectonic geomorphology of the Hoyran Graben (Western Anatolia, Türkiye): insights from geomorphic indices

Yaren Sena ÇETİN<sup>1</sup>, Hasan Salih AĞAR<sup>2</sup>, Burcu KAHRAMAN<sup>2</sup>, Levent BAYRAM<sup>2</sup>, Ahmet Özkan KUL<sup>3</sup>, Erman ÖZSAYIN<sup>2</sup>, \* and Serkan ÜNER<sup>3</sup>

<sup>1</sup> Hacettepe University, Graduate School of Science and Engineering, TR-06800, Ankara, Türkiye. ORCID: 0000-0001-6801-1804 [Y.S.Ç.]

<sup>2</sup> Hacettepe University, Department of Geological Engineering, TR-06800, Ankara, Türkiye. ORCID: 0009-0006-8666-5186 [H.S.A.], 0000-0003-4172-5086 [B.K.], 0000-0002-6197-4330 [L.B.], 0000-0003-3948-5482 [E.Ö.]

<sup>3</sup> Van Yüzüncü Yıl University, Department of Geological Engineering, TR-65080, Van, Türkiye. ORCID: 0000-0003-1854-2206 [A.Ö.K.], 0000-0001-5974-1856 [S.Ü.]



Çetin, Y.S., Açar, H.S., Kahraman, B., Bayram, L., Kul, A.Ö., Özsayın, E., Üner, S., 2024. Tectonic geomorphology of the Hoyran Graben (Western Anatolia, Türkiye): insights from geomorphic indices. *Geological Quarterly*, 68: 1; <https://doi.org/10.7306/gq.1724>

Associate Editor: Paweł Aleksandrowski

The area between Western Anatolia and Isparta Bend comprises numerous depressions and the active faults that bound them. The Hoyran Graben is one of these depressions, located at the northernmost part of the Isparta Bend. This NE–SW-oriented graben is bounded by the Hoyran Fault in the northwest and the Uluborlu, Senirkent and Kumdanlı faults in the south-east, respectively. We evaluate the seismic activity potential among segments of the boundary faults in the light of fieldwork and morphometric indices. These boundary faults of the Hoyran Graben are divided into twelve segments for the analysis, with indices used including mountain-front sinuosity (*Smf*: 1.05–2.02), valley floor width-to-valley height ratio (*Vf*: 0.11–1.34), hypsometric curve and integral (*Hi*: 0.4–0.73), asymmetry factor (*Af*: 13.76–87.03), stream length-gradient (*SL*: 1.48–9450) and normalized channel steepness (*Ksn*: 2.38–990.38). The results obtained, together with field observations, indicate that the Uluborlu, Senirkent and Kumdanlı faults, as well as the western segments of the Hoyran Fault, represent higher potential in terms of seismic activity with uplift rates >0.5 mm/y, while the central and eastern segments show moderate activity with uplift rates between 0.05 and 0.5 mm/y. Thus, the boundary faults of the Hoyran Graben need further attention in terms of regional seismic hazard.

Key words: seismic activity, boundary faults, morphometric analysis, palaeostress analysis, seismic hazard.

### INTRODUCTION

Morphometric analysis is one of the most significant methods used to investigate the interaction between tectonics and drainage network quantitatively, to compare the relative activities among fault segments in terms of their seismic potential (Keller and Pinter, 2002). In recent years, studies on revealing such relative activities among segments of seismogenic faults via morphometric indices has come increasingly into prominence. The Acambay Graben (Ramírez-Herrera, 1998), the Sierra Nevada (Pérez-Peña et al., 2010), the Sierra Cabrera (Giaconia et al., 2012), the Honaz Fault (Özkaymak, 2014), the

Tuz Gölü Fault Zone (Yıldırım, 2014), the Çameli Basin (Özsayın, 2016), the Lake Van Basin (Sağlam-Selçuk, 2016), and the Malatya Fault (Zabcı, 2020) represent some of these studies, where several geomorphological indices were applied to compare responses of landforms to seismically active fault segments. The most reliable and common tools comprise the mountain-front sinuosity, valley floor width-to-valley height ratio, asymmetry factor, hypsometric curve and integral, stream length gradient and normalized channel steepness indices.

The Western Anatolia Province is one of the most rapidly extending areas in the world, at 20 mm/y (Reilinger et al., 1997). This extension creates high frequency seismicity generated by the boundary faults of dissimilarly-oriented horst-graben systems (Eyidoğan and Jackson, 1985; Ambraseys, 1988; Eyidoğan, 1988; Jackson and McKenzie, 1988; Jackson et al., 1992; Taymaz, 1993; Ambraseys and Jackson, 1998; Aktuğ et al., 2009). This region is limited by the Isparta Bend in the east, located in central Anatolia (Uysal et al., 1980; Kissel and Pois-

\* Corresponding author: e-mail: eozsayin@hacettepe.edu.tr

son, 1987; Kissel et al., 1993; Morris and Robertson, 1993; Piper et al., 2002; Özsayın and Dirik, 2011; Fig. 1A). Such horst-graben structures, developing in a radial pattern on the upper part of the Isparta Bend, display unique morphological and structural features (Emre et al., 2003). The Hoyran Graben is situated at the north of this structure and it is bounded by seismically active normal faults (Fig. 1B). Several studies were performed around the western part of the Isparta Bend in terms of its tectonic evolution (e.g., Koçyiğit, 1981; Waldron, 1982) and seismicity of the region (e.g., Taymaz and Price, 1992; Emre et al., 2003; Özalp et al., 2018; Kürçer et al., 2021). However, none of these investigated the seismic activity potential among the fault segments of the Hoyran Graben. Besides, the limited numbers of earthquakes, dispersed along different fault segments, complicate the understanding of the possible seismic gaps between them.

Therefore, this study: (i) evaluates the fault segments of the Hoyran Graben using geomorphic indices, as well as field observations; (ii) reveals the seismic activity potential among the fault segments.

## GEOLOGICAL SETTING

### WESTERN ANATOLIA

The Anatolian plate, moving westwards along the North and East Anatolian Fault systems, is rotating counter-clockwise and obducting onto the African plate in the SW along the Aegean-Cyprian arc (McKenzie, 1978; Şengör, 1979; Jackson and McKenzie, 1984; Şengör et al., 1985; Le Pichon et al., 1995; Fig. 1A). This situation also controls strongly N–S-oriented continental extension in Western Anatolia (Le Pichon and Angelier, 1979; Şengör et al., 1984; Reilinger et al., 2010).

The origin of continental extension in the Western Anatolia region has been debated many times and various models have been proposed. They include: (i) tectonic escape (e.g., Şengör and Yılmaz, 1981; Şengör et al., 1985; Görür et al., 1995), (ii) back-arc spreading (e.g., McKenzie, 1978; Le Pichon and Angelier, 1979; Meulenkaamp et al., 1988; Jolivet et al., 1998), (iii) orogenic collapse (e.g., Dewey, 1988; Seyitoğlu and Scott, 1991, 1992; McClusky et al., 2000), (iv) an episodic two-stage graben (e.g., Bozkurt and Park, 1994; Koçyiğit et al., 1999; Yılmaz et al., 2000; Sözbilir, 2001; Bozkurt and Rojay, 2005), (v) velocity difference (e.g., Doglioni et al., 2002), (vi) divergent extension (e.g., Hetzel et al., 1995) and (vii) slab-tearing and trench-retreat models (e.g., Brun and Sokoutis, 2010; Jolivet and Brun, 2010; Jolivet et al., 2013; Karaoğlu and Helvacı, 2014). Additionally, several evolutionary models combining the basic types listed above have been suggested for different time intervals in the western Anatolia region (e.g., Sözbilir, 2002; Westaway, 2003; Kaya et al., 2004; Agostini et al., 2010; Gürer et al., 2013).

The eastern margin of the Western Anatolian Extensional Province also includes the regional-scale structure known as the Isparta Bend, where the study area is located (Fig. 1A). This is a V-shaped morphotectonic structure (~180 km long N–S and ~100 km wide E–W), which is situated to the north of Antalya Bay. The first attempt to explain its origin, initially defined and reported by Blumenthal (1951), was made by Dumont (1976). The Isparta Bend is bounded to the west by the NE-trending Fethiye-Burdur and to the east by the NW-trending Akşehir Fault zones (e.g., Barka et al., 1995; Koçyiğit et al., 2000; Fig. 1A). Later studies also discuss the existence (Kaymakçı et al., 2017) and characteristics of the Fethiye-Burdur Fault Zone (e.g., Elitez and Yaltrak, 2014; Alçiçek, 2015).

Earlier research identified three main nappe sheets as essential components, formed as linear features in the Isparta Bend. The initial sheet comprises the Antalya Nappe units, originating from the southern part of the Neotethys. These units were thrust onto the Tauride carbonate platform (Anamas-Akseki Autochthon) in the late Early Paleocene (Uysal et al., 1980; Balci, 2011a, b). The second one comprises the Beyşehir-Hoyran-Hadım Nappe units, derived from the northern branch of the Neotethys. These were emplaced onto the central Tauride platform in two consecutive stages (Campanian and Late Lutetian; Piper et al., 2002). The Lycian Nappe units share the same origin as the Beyşehir-Hoyran-Hadım Nappe units and underwent a two-stage emplacement onto the western Tauride platform (Late Oligocene-Late Langhian; Piper et al., 2002). Palaeomagnetic studies indicated a 40° clockwise rotation for the eastern part of the Isparta Bend (Kissel et al., 1993), while a 30° counter-clockwise rotation was calculated for the western part (Kissel and Poisson, 1987; Morris and Robertson, 1993). Notably, palaeomagnetic studies do not indicate any rotation from the Pliocene to recent times for the central part of the Isparta Bend (Kissel and Poisson, 1987).

The extension in Western Anatolia created numerous basins between the Aegean Sea and the Isparta Bend. Generally, they were controlled by active faults, and include the E–W-trending Büyük Menderes and Küçük Menderes, the NE-trending Hoyran, Baklan, Burdur and Acıgöl, and the NW-trending Gediz and Dinar grabens (Fig. 1B). Seismic studies and geodetic velocity measurements demonstrate that the region is deformed by high strain rates along these active faults, generating high-frequency seismicity (e.g., Barka and Reilinger, 1997; Kahle et al., 1998; Kurt et al., 1999; Özener et al., 2013; Dođru et al., 2014).

### HOYRAN GRABEN

Previous studies indicate that the strain related with the convergence between African and Eurasian plates was divided between the subduction zone and the plate above. This interplay led transitions from thin- to thick-skinned thrusting, accompanied by reactivation of former segments within the nappe stacks (e.g., Faccenna et al., 2014). Consequently, this phenomenon created strongly curved mountain ranges and related continental areas of extension (e.g., Van Hinsbergen et al., 2020). In the early Miocene, depressions such as the Hoyran, Akşehir, Beyşehir, Burdur and Eğirdir basins (Fig. 1B) formed due to tectonic uplift in the Western Taurus Mountains (Karaman, 2010). The development of these basins, which are bordered by active faults of various orientations, is explained by counter-clockwise rotation of the area west of the Isparta Bend (Kissel and Poisson, 1987; Morris and Robertson, 1993; Karaman, 2010). These basins were infilled by lacustrine deposits from the Miocene.

The NE-trending Hoyran Graben is one of these grabens, located in the northern part of the Isparta Bend (Fig. 1B). The graben is ~80 km long and 20 km wide. Earlier studies suggest that this graben was formed as a N–S oriented basin as a consequence of N–S-trending contraction between the African and Eurasian plates which created an ~E–W oriented tensional stress regime during the Middle Miocene. Later, this graben was cut by the Fethiye-Burdur Fault Zone and took its present-day geometry together with the counter-clockwise rotation of the western limb of the Isparta Bend (e.g., Karaman, 2010).

The rock units outcropping in the Hoyran Graben are divided into two main successions, as basement units and graben-fill. The oldest basement unit in the area is the Paleozoic Anamas-Akseki Autochthon that has undergone low-grade metamorphism. It was first named as the Seydişehir

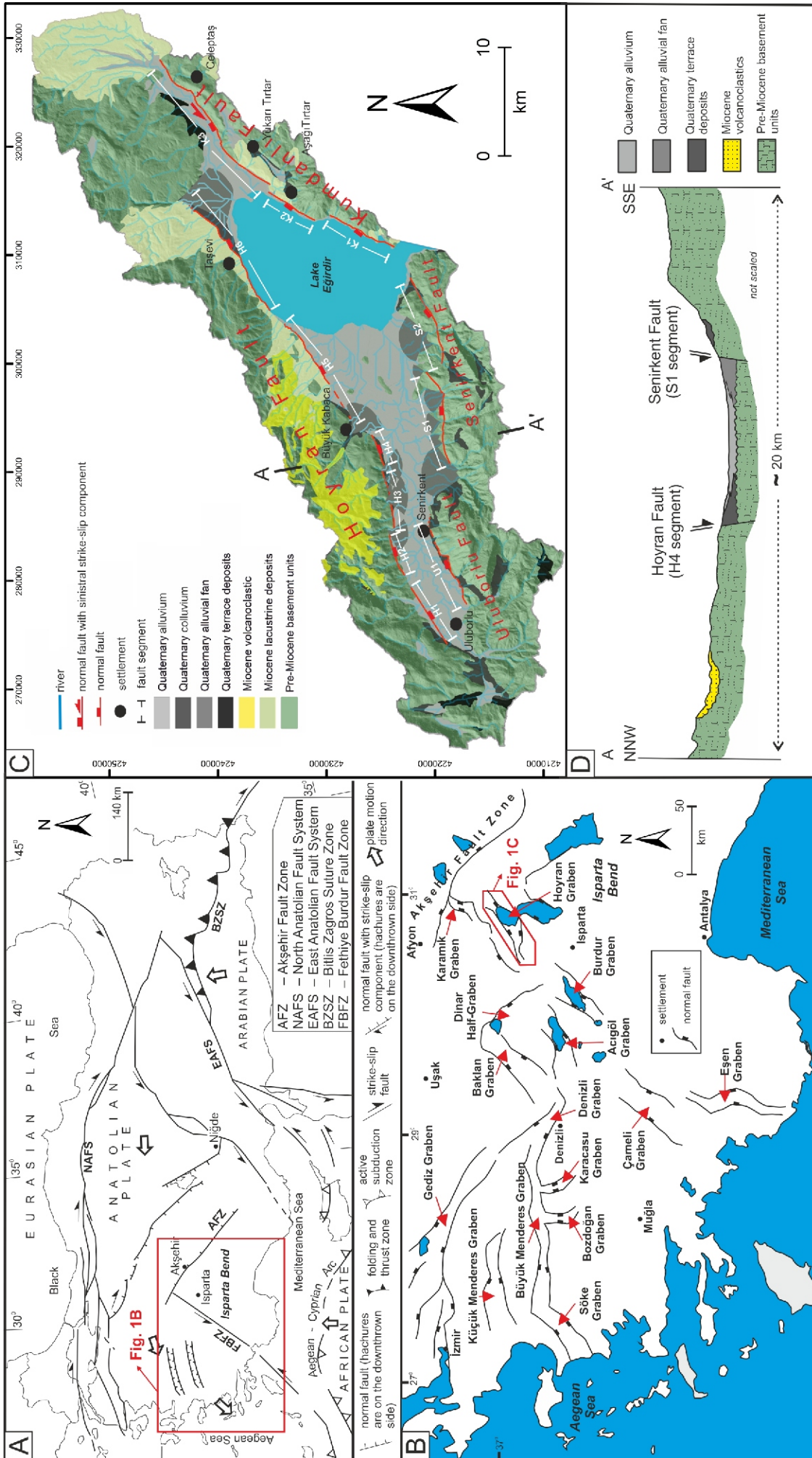


Fig. 1. Neotectonics of the study area within the Anatolian Plate

schists by [Blumenthal \(1947\)](#) and consists of metasiltstone, metashale and metasediments intercalated with light green, grey and locally reddish-blue quartzite with red and pink nodular limestone in its lower levels. Due to the onset of greenschist metamorphism, the matrix has become chloritized and sericitized. Grading and cross-bedding is observed in the metasediments. Green, altered volcanic sills intrude the lower levels of the formation ([Balci, 2011a, b](#)). These units are tectonically overlain by ultramafic rocks, containing peridotite, serpentinite, harzburgite, gabbro and diabase of an ophiolitic mélange (Beyşehir-Hoyran-Hadım Nappes) ([Şenel et al., 1981; Öztürk and Öztürk, 1989](#)). Platform carbonates of the Lycian Nappes, represented by pelagic limestone intercalations, and oolitic and oncoidal limestones containing benthic foraminifera, also constitute basement rocks ([Balci, 2011a, b](#)). The last basement unit, of Upper Paleocene-Eocene flysch deposits, was defined by [Özgül et al. \(1991\)](#). This unit, ~1000 m thick, comprises basal beige and red, thin-bedded micritic limestones passing upwards into thin- to medium-bedded, grey, green, beige calcarenites, micrites, clayey and sandy limestones interbedded with sandstones, claystones, siltstones and conglomerates.

Basin-fill deposits rest unconformably on these basement units. They begin with Upper Miocene-Pliocene pale grey-beige, thin- to medium-bedded marl and green claystone. Among these units, beige, poorly sorted, carbonate- or clay-cemented conglomerate lenses can be observed. The clasts are of volcanic rock, limestone, serpentine, quartz and radiolarite. This level is overlain by yellow-beige, thin-to medium-bedded gastropod-bearing lacustrine limestones intercalated with claystones and marls. These units are overlain by tuffaceous sandstones, limestones, basalts and andesites. This sequence is between 200 m and 1200 m thick ([Öztürk and Öztürk, 1989; Balci, 2011a, b](#)) and is unconformably overlain by Quaternary clastic deposits ([Fig. 1C, D](#)).

The graben is bounded by the Hoyran Fault to the north and by the Uluborlu, Senirkent and Kumdanlı faults to the south ([Fig. 1C, D](#)). The 45 km long and N55°E trending fault, extending between Uluborlu and Aşağı Kaşıkara, is named as the Hoyran Fault for the first time on the basis of fault-slip data in this study. This tectonic structure is morphologically distinctive between Büyükkabaca and Taşevi, and possibly active, from the distribution of earthquake epicentres. The fault is divided into six segments for geomorphic analysis according to their position and step-over zones: H1–H6. The H1 segment is 7 km long and bounds basement units with Quaternary colluvium and alluvium. It constitutes the western part of the Hoyran Fault. The next segment (H2) is 4 km long and juxtaposes basement units with Quaternary alluvium. H3, 6 km long, is east of H2 and separates basement units from Quaternary colluvium, as does H4, 3 km long. H5 is 11 km long and juxtaposes Miocene lacustrine deposits with Quaternary colluvium and alluvium. H6 is 13 km long and bounds Miocene lacustrine deposits with Quaternary colluvium, forming the easternmost part of the Hoyran Fault.

The Uluborlu Fault was defined by [Emre et al. \(2013\)](#) as a Holocene fault, being dip-slip and normal. The general trend of the fault is N65°E with NW-dipping fault planes. It forms the contact between Quaternary alluvium in the north and the Mesozoic limestones in the south. As this fault was mapped as a single segment by [Emre et al. \(2013\)](#), the name "U1" is given for geomorphic analysis. It is ~10 km long and lies between Uluborlu and Senirkent ([Fig. 1C](#)).

The Senirkent Fault, identified by [Şaroğlu et al. \(1987\)](#), is 20 km long. It extends from the east of Senirkent to the southern part of Lake Eğirdir. According to [Emre et al. \(2013\)](#), it is a normal, dip-slip Quaternary fault, generally striking N75°E with NNW-dipping planes. The Senirkent Fault is divided into two segments, S1 and S2, which are consistent with those identified by [Emre et al. \(2013\)](#). Both segments are ~9 km long and juxtapose basement units with Quaternary colluvium. Alluvial fans, hanging valleys, and old terraces are commonly observed along these all segments ([Fig. 2](#)).

The Kumdanlı Fault was firstly defined by [Koçyiğit \(1983\)](#) as the Gökçeali Fault. However, this fault was termed as the Burdur-Hoyran Fault ([Karaman, 1988, 1989; Yağmurlu, 1991](#)) and the Kumdanlı Fault ([Şaroğlu et al., 1992](#)). In this study, the "Kumdanlı Fault" is used to preserve consistency and clarity of description. The Kumdanlı Fault is 27 km long and defined as a Holocene fault with N50°E strike and NW-dipping planes on the updated Active Fault Map of Türkiye ([Emre et al., 2013; Fig. 3A, B](#)).

Fault planes observed in the north of Celeptaş have a normal fault character with a sinistral strike-slip component ([Fig. 3C, D](#)). This structure is divided into three segments, namely K1, K2, and K3. The segment K1 is the western one, ~6 km long, and juxtaposes basement units and Miocene lacustrine deposits with Quaternary units. The K2 segment, 8 km long, lies between Aşağı Tirtar and Celeptaş, and also cuts the basement and the Miocene lacustrine deposits. K3 is the easternmost segment, ~12 km long and separating basement units and Miocene lacustrine deposits from Quaternary alluvium.

The study area is called the "Turkish Lakeland". In this region, there are several terminal lakes of various dimensions, most of which are bounded by active faults. Lake Eğirdir is one of these lakes and is positioned at an elevation of 915 m a.s.l. The northern part of this lake is located in the Hoyran Graben. This part of the lake is bounded by the H6 segment of the Hoyran Fault to the northwest, and the K1 and K2 segments of the Kumdanlı Fault to the southeast ([Fig. 1C](#)).

## MATERIAL AND METHODS

In this study, 30 m Shuttle Radar Topographic Mission (SRTM) digital elevation model (DEM) data (available at <https://earthexplorer.usgs.gov>) were used to evaluate the geomorphic indices for the Hoyran Graben. The drainage sub-basins and river network of the region were drawn using *ArcGIS® Desktop Arcmap (v.10.8)* on the DEM provided. Possible gaps in the DEM were filled through interpolation (Fillmed tool) to obtain a homogeneous data set. The drainage basins and river network of the region were extracted from the DEM with related tools (Flowdir and Flow acc tools) with the D8 algorithm and these river networks were compared with the networks on the topographic maps. A total of 12 fault segments were defined in relation to their positions and/or step-over zones as defined by [Biddle and Christie-Blick \(1985\)](#) and [Peacock et al. \(2000\)](#), and 84 drainage sub-basins controlled by these segments were determined for the calculations. Active tectonics and rock units directly control morphological features such as drainage pattern, stream gradient, mountain front geometry, and erosional processes. In this study, seven geomorphic indices were used in the light of previous studies which were applied to several regions, showing similar geological and structural contents (e.g., [Azañón et al., 2015; Sağlam-Selçuk, 2016; He et al., 2018; Valkanou et al., 2020](#)). These are the hypsometric curve and integral, mountain-front

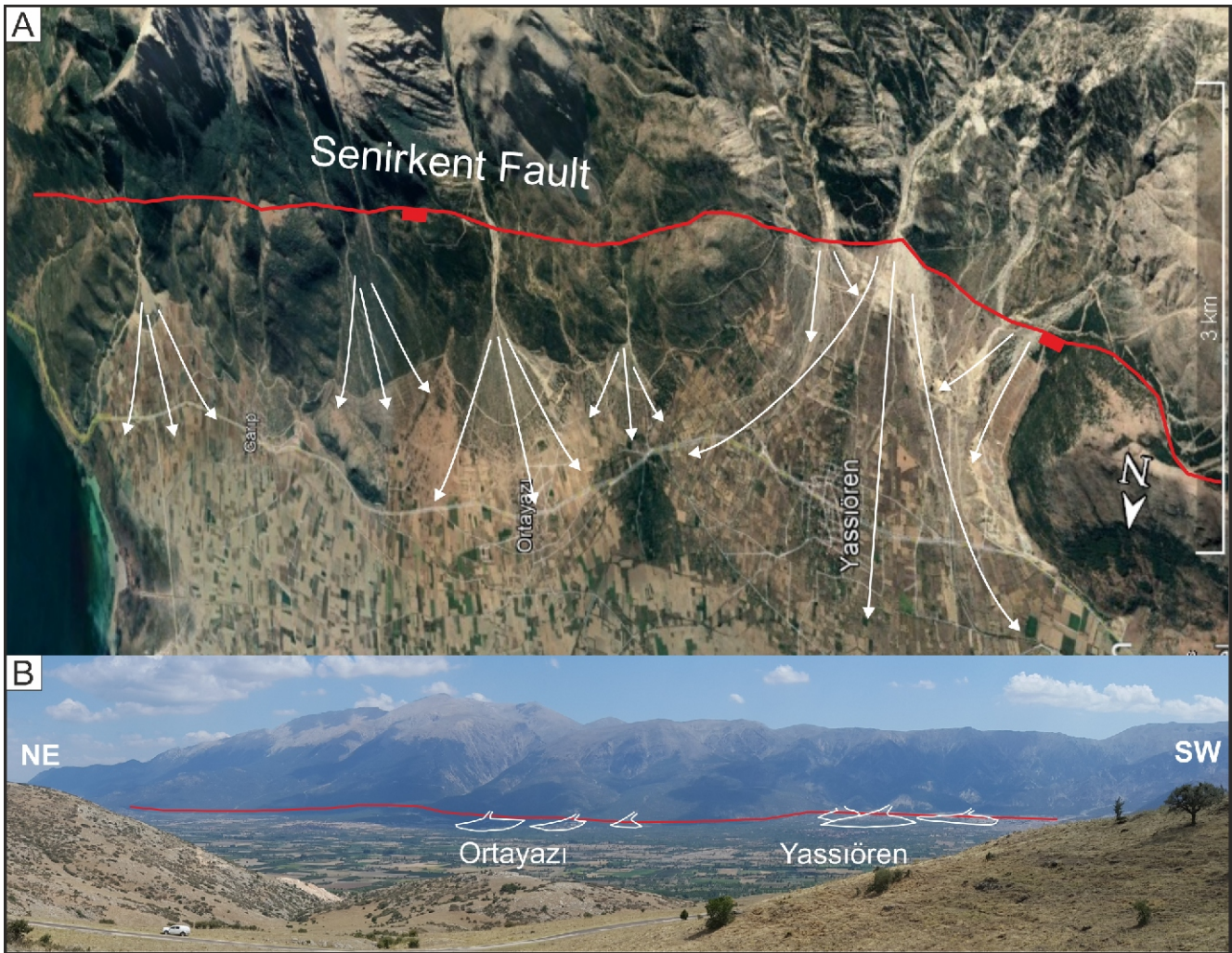


Fig. 2. Alluvial fans set along the Senirkent Fault

A – Google Earth image; B – field view

sinuosity, valley floor width-to-valley height ratio, drainage basin asymmetry, stream length-gradient and normalized channel steepness indices (Fig 4).

Mountain-front sinuosity ( $S_{mf}$ ) is a tool for expressing the balance between tectonic activity and erosional forces. Straight mountain-fronts (low  $S_{mf}$  values) are obtained when high tectonic activity and related uplift overcome erosional processes. When tectonic activity is low, erosional processes create more sinusoidal mountain-fronts (high  $S_{mf}$  values; Keller and Pinter, 2002; Fig 4).

$V_f$  is a useful tool for evaluating valley incision and shape between fault segments. Higher tectonic activity and related uplift rates will reveal deeply incised, V-shaped valleys (lower  $V_f$  values). By contrast, in erosion-dominated areas, the valleys are broad- and flat-floored (higher  $V_f$  values) (Bull and McFadden, 1977; Keller and Pinter, 2002; Fig 4).

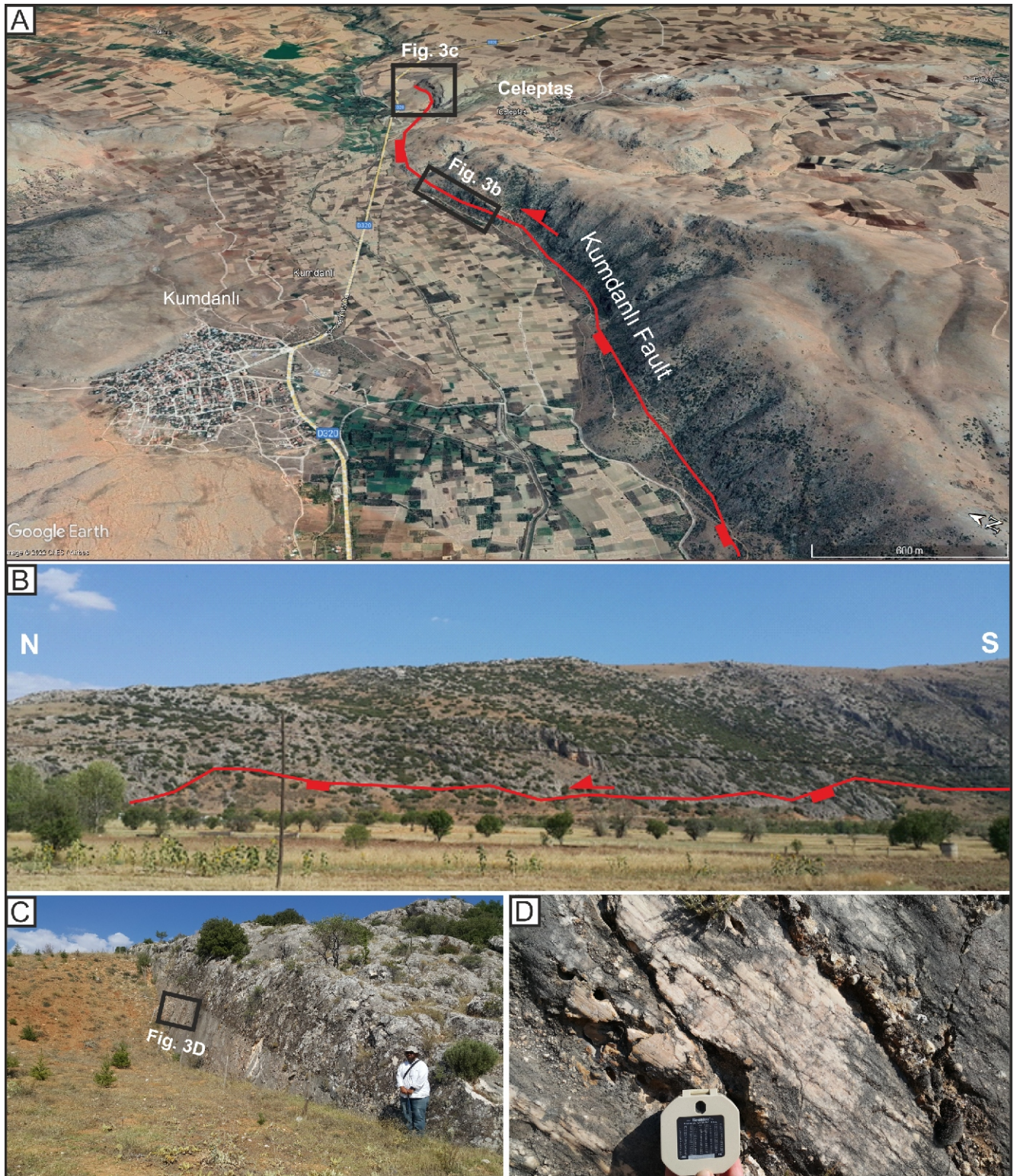
$SL$  describes the stream-channel slope along the river bed and indicates unexpected slope changes owing to erosional dissimilarities among lithological boundaries and/or faults. A gentle slope along the river bed gives low  $SL$  values whereas sharp drops generate high values (Keller and Pinter, 2002).

$K_{sn}$  controls slope gradient anomalies along the river channels (Ouimet et al., 2009; Whittaker, 2012). In a drainage basin, the slope of the river bed gradually decreases downwards. This

situation can be changed by lithological boundaries due to rock resistance to erosion or by active faulting, generating vertical displacement. The exponential relationship between channel slope ( $S$ ) and upstream area ( $A$ ) in graded rivers are defined as a power-law (Hack, 1957), stated by:

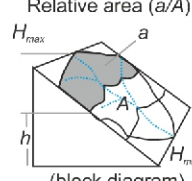
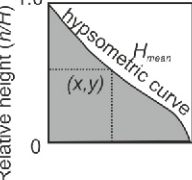
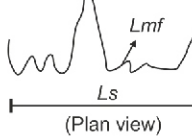
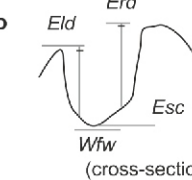
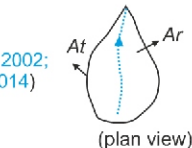
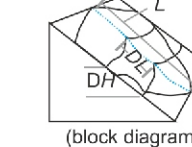
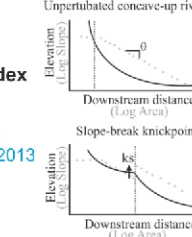
$$S = K_s A^{-n}$$

In this formula,  $K_s$  represents the channel steepness-index and  $n$  refers to the concavity index (Flint, 1974). Disparities as active tectonics, climate and river-bed lithology directly disturb the slope of the channel and upstream area, shifting the  $K_s$  and  $n$  in the equation (Wobus et al., 2006; Kirby and Whipple, 2012). For the determination of  $K_s$  and  $n$  in a river profile, regressions are executed in logarithmic slope-area plots (Ferrater et al., 2015). These plots can be used to locate knickpoints and distinct areas of different uplift (Wobus et al., 2006; Kirby and Whipple, 2012; Burbank and Anderson, 2013; Whipple et al., 2013). These knickpoints occur due to constant changes that happen in boundary conditions as base-level falls according to uplift-rate changes or variations in climatic conditions (Snyder et al., 2003; Bishop et al., 2005; Kirby and Whipple, 2012). The concavity index ( $n$ ) ranges between 0.4 and 0.6 in most situa-



**Fig. 3. The Kumdanlı Fault between Kumdanlı and Celeptaş**

**A** – Google Earth image; **B** – slope-breaks along the Kumdanlı Fault; **C** – fault plane observed to the north of Celeptaş; **D** – close-up view of the fault plane and slickenlines

Morphometric parameter and mathematical derivation	Measurement procedure	Explanation and activity classes
<p><b>HI – hypsometric integral</b>  <math>HI = (h_{mean} - h_{min}) / (h_{max} - h_{min})</math>                      (Keller and Pinter, 2002)</p>	 <p>Relative area (<math>a/A</math>)                      (block diagram)</p>	<p>Known as basin-area altitude distribution and defined as the area under the hypsometric curve. Higher values of <math>HI</math> indicate that most of the topography is high relative to the mean. Intermediate (straight or S-shaped curves) to low (upwardly concave curves) values are associated with more evenly dissected drainage basins.</p>
<p><b>Hypsometric curve</b>  <math>x = a/A</math>  <math>y = h/H</math>                      (Keller and Pinter, 2002)</p>	 <p>Relative height (<math>h/H</math>)                      hypsometric curve                      (x,y)                      1.0                      0</p>	<p>Describes the distribution of elevations across an area of land. Convex hypsometric curves characterise relatively 'young' weakly eroded regions, S-shaped curves characterise moderately eroded regions, and concave curves characterise relatively 'old' highly eroded regions.</p>
<p><b>S<sub>mf</sub> – mountain front sinuosity</b>  <math>S_{mf} = L_{mf}/L_s</math>                      (Bull, 1977; Bull and McFadden, 1977; Rockwell et al., 1984; Keller and Pinter, 2002; Silva et al., 2003; El Hamdouni et al., 2008)</p>	 <p>(Plan view)</p>	<p>Reflect a balance between the tendency of stream and slope processes to produce irregular (sinuous) mountain front and vertical active tectonics that tend to produce a prominent straight front.</p>
<p><b>V<sub>f</sub> – valley floor width-to height ratio</b>  <math>V_f = 2V_{fw} / [(Eld - Esc) + (Erd - Esc)]</math>                      (Bull and McFadden, 1977; Keller and Pinter, 2002; Silva et al., 2003)</p>	 <p>(cross-section)</p>	<p>Define the ratio of the width of the valley floor to the mean height of two adjacent divides. The index reflects differences between broadfloored canyons with relatively high values of <math>V_f</math>, and V-shaped canyons with relatively low <math>V_f</math> values.</p>
<p><b>AF – asymmetry factor</b>  <math>AF = 100 (A_r / A_t)</math>                      (Hare and Gardner, 1985; Keller and Pinter, 2002; Özkaymak and Sözbilir, 2012; Özkaymak, 2014)</p>	 <p>(plan view)</p>	<p>Define the ratio of the area of the basin to the right (<math>A_r</math>) of the trunk stream to the total area of the drainage basin (<math>A_t</math>). The index was determined to detect tectonic tilting transverse to the flow at drainage basins.</p>
<p><b>SL – stream length-gradient index</b>  <math>SL = (DH/DL)L</math>                      (Hack, 1973; Keller and Pinter, 2002; El Hamdouni et al., 2008; Alipoor et al., 2011)</p>	 <p>(block diagram)</p>	<p>Total or available stream power is related to the slope of the water channel. Sudden changes in <math>SL</math> values along the stream channel indicate lithological differences and/or possible tectonic activity</p>
<p><b>K<sub>sn</sub> – normalized channel steepness index</b>  <math>S = k_{sn} A^{-\theta}</math>                      (Wobus et al., 2006; Kirby and Whipple, 2012; Whipple et al., 2013; Burbank and Anderson, 2013; Bellin et al., 2014; Scotti et al., 2014)</p>	 <p>Unperturbed concave-up river                      Elevation (Log Slope)                      Downstream distance (Log Area)  <math>\theta</math>                      Slope-break knickpoint                      Elevation (Log Slope)                      Downstream distance (Log Area)  <math>k_{sn}</math></p>	<p>Define the channel slope if it is unexpectedly steep or gentle with respect to its drainage area. Normally, the channel slope decreases with drainage area. Existing of knickpoints show sudden increases along slope profiles that may be related to lithological changes and/or tectonic uplift.</p>

$L_{mf}$  – length of mountain front along the mountain-piedmont junction;  $L_s$  – straight-line length of the front;  $V_{fw}$  – width of valley floor;  $Eld$  and  $Erd$  – respective elevations of the left and right valley divides;  $Esc$  – elevation of the valley floor;  $x$  and  $y$  – axes;  $a$  – surface area within the basin above a given line of elevation;  $A$  – total surface area of the basin;  $h$  – given line of elevation;  $H_{mean}$  – mean elevation;  $H_{min}$  – minimum elevation;  $H_{max}$  – maximum elevation;  $DH$  – change in elevation of the reach;  $DL$  – length of the reach;  $L$  – total channel length from the point of interest where the index is being calculated upstream to the highest point on the channel;  $S$  – channel slope;  $A$  – upstream area;  $K_{sn}$  – normalized channel steepness index;  $\theta$  – concavity index

**Fig. 4. Summary of the morphometric parameters used to evaluate relative tectonic activity among the boundary faults of the Hoyran Graben (from Özkaymak, 2014; Özsayın, 2016; Özsayın et al., 2023)**

tions and is relatively unaffected by active tectonics, lithological and/or climatic changes (Kirby and Whipple, 2012; Whipple et al., 2013). The “normalized” steepness index ( $K_{sn}$ ) is used for river reaches of static “reference” concavity (Wobus et al., 2006), used in morphometric studies (e.g., Wobus et al., 2006; Kirby and Whipple, 2012; Whipple et al., 2013; Ferrater et al., 2015; Camafort et al., 2020; Sağlam-Selçuk and Kul, 2021). Therefore, the value is accepted as 0.5 during the calculations in TecDEM toolbox analysis (Fig 4).

The drainage basin asymmetry factor ( $AF$ ) was developed to detect the tilting of small-scale drainage basins due to active tectonics. This factor permits resolution of the overall tilt of the basin landscape regardless of whether the tilt is local or regional (Hare and Gardner, 1985). If the  $AF$  is higher than 50, the main channel has moved to the downstream left-hand side of the drainage basin. If the  $AF$  is less than 50, the channel has shifted to the downstream right-hand side of the drainage basin (Hare and Gardner, 1985).

Fault-slip data from different segments of the faults were collected in the field for palaeostress analysis. *Win-Tensor* (v.5.9.3) software, developed by Damien Delvaux, was used to evaluate 34 kinds of fault-slip data from the fault planes where the fault type can be determined.  $R$  values of each palaeostress analysis, which indicates the shape of the stress ellipsoid that will occur depending on the positioning of the principal stress axes, were used to express the peripheral conditions that the faults reflect. According to the  $R$  values, the tensional stress field ( $\sigma_1$  vertical) can be radial tension ( $0 < R < 0.25$ ), pure tension ( $0.25 < R < 0.75$ ) or transtension ( $0.75 < R < 1$ ). For the strike-slip stress field ( $\sigma_2$  vertical), the  $R$  values vary as pure strike-slip ( $0.25 < R < 0.75$ ), transtension ( $0.75 < R < 1$ ) and transpression ( $0 < R < 0.25$ ), and for the compressional stress field ( $\sigma_3$  vertical) it may reflect radial compression ( $0.75 < R < 1$ ), pure compression ( $0.25 < R < 0.75$ ) or transpression ( $0 < R < 0.25$ ; Delvaux et al., 1997; Delvaux and Sperner, 2003). Faults that were considered to be products of different tectonic regimes due to their relations in the field were evaluated separately. Moreover, the *Win-Tensor* software also indicates un-conformable fault-slip data, resulting from different stress regimes. Thus, these fault-slip data were removed from the analysis and the stresses were recalculated.

## RESULTS

### FIELD OBSERVATIONS AND PALAEOSTRESS ANALYSIS OF THE FAULT-SLIP DATA

In order to determine the fault characteristics and their related morphological features, field studies along the margins of the Hoyran Graben were performed in this research. The southeastern margin of the graben is bounded by the Uluborlu, Senirkent and Kumdanlı faults from west to east, respectively. The Hoyran Fault forms the northwestern margin of the Hoyran Graben.

The Uluborlu Fault represents sharp topographic slope-breaks with linear mountain-fronts. Small alluvial fans are aligned along the fault. Rivers cut the Uluborlu Fault perpendicularly and none of them are offset by faulting (Fig. 1C). Most of the fault planes are covered with the Quaternary colluvium deposits.

The Senirkent Fault constitutes the central part of the southern margin and offsets it ~3 km to the SE of the Uluborlu Fault in the eastern part of Senirkent. This fault shows sinusoidal mountain-fronts with respect to the Uluborlu Fault. Well-developed, larger alluvial fans are aligned along it (Figs. 1C and 2).

General trend of the Senirkent Fault immediately changes at the mountain pass of Lake Eğirdir and continues as the Kumdanlı Fault, which limits the northern part of the lake to the SE and forms the southeasternmost part of the graben. The western part of the Kumdanlı Fault is covered by the lake, and its linear shoreline coincides with the fault. In this section, only a linear drainage pattern, perpendicular to the shoreline, can be seen. In the eastern part, along the Kumdanlı Fault, sinusoidal mountain-fronts can be traced, where a limited number of fault planes juxtapose the basement units with Quaternary alluvium (Figs. 1C and 3).

By contrast, the western part of the Hoyran Fault represents linear mountain-fronts and sharp topographic slope-breaks. In this area, the basement units juxtapose with Quaternary alluvium and colluvium. Alluvial fans, located in the central part, are characteristic of this section. The central to eastern part of the Hoyran Fault exhibits sinusoidal mountain-fronts and incised river profiles. The Miocene units also juxtapose with Quaternary alluvium and colluvium along the fault, with larger alluvial fans. This section reflects the flat topography compared to other parts of the study area (Fig. 1C).

A total of 34 kinds of fault-slip data from available fault planes were measured at three locations to calculate principal stress orientations. The measurements were taken from the U1 segment of the Uluborlu Fault, the H2 segment of the Hoyran Fault, and the K3 segment of the Kumdanlı Fault. The analysis of fault-slip data collected from U1 represents pure tension, while the H2 and K3 segments show a radial tensional stress tensor with  $N52^\circ W$ ,  $N13^\circ W$  and  $N79^\circ W$  orientations, respectively (Fig. 5 and Table 1).

## GEOMORPHIC INDICES

### HYPSONETRIC CURVE AND INTEGRAL (HC-HI)

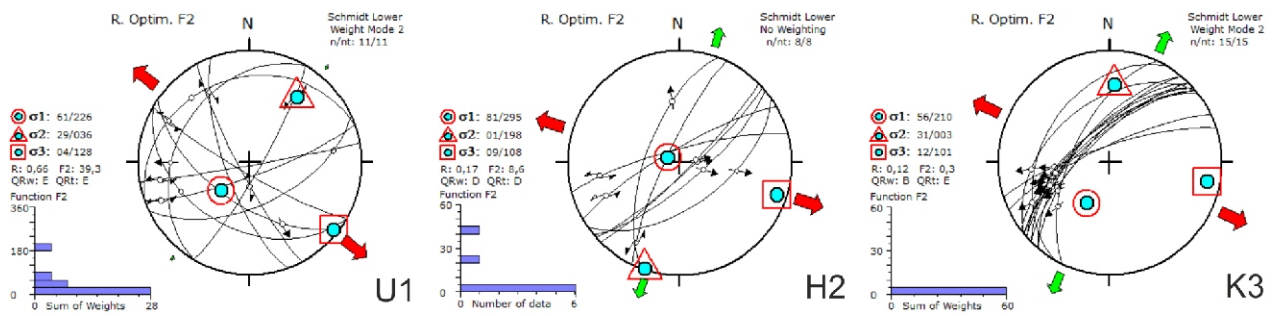
The hypsonetric curves of the drainage sub-basins, controlled by 12 fault segments in the Hoyran Graben, were calculated and divided into three groups. Convex curvature, indicating relatively high tectonic activity, was obtained from the U1 (1), S1 (3), K3 (3), H5 (1, 7, 8, 9, 10, 11), H6 (1, 3, 5, 9, 17, 18) segments. S-shaped or linear results, showing moderate activity, were determined from the U1 (8, 9, 10, 11, 12), S1 (2, 4), S2 (5), K3 (1, 4), H1 (1, 3, 5), H3 (4, 5), H4, H5 (2, 4, 5, 6), H6 (2, 4,

Table 1

Chart showing the principal stress axis and  $R$  values evaluated for the U1, H2, and K3 segments

Location	Fault type	Number of slip data	1	2	3	R
U1 segment	Oblique-slip	11	61/226	29/036	04/128	0.66
H2 segment	Oblique-slip	8	81/295	01/198	09/108	0.17
K3 segment	Oblique-slip	15	56/210	31/003	12/167	0.12





**Fig. 5.** Stereographic plots of fault-slip data collected from the U1, H2 and K3 segments on a Schmidt lower hemisphere, where  $\sigma_1$ ,  $\sigma_2$  and  $\sigma_3$  are principal, intermediate and least stress axes, respectively, which are obtained using *Win-Tensor* (v.5.9.3) software (Delvaux et al., 1997; Delvaux and Sperner, 2003) (red arrows show primary horizontal component of extensional deviatoric stress while green arrows show alternate components)

6, 8, 12, 13, 15) segments. The remaining sub-basins, representing concave curvature, represent highly eroded regions (Fig. 6).

Mean *HI* values of sub-basins controlled by each segment range between 0.40 and 0.73 (Fig. 7 and Table 2). The highest values ( $> 0.5$ ) were obtained from the U1, S1, S2, K1, K2, K3, H3, H5 and H6 segments, and moderate values ( $0.4 < HI < 0.5$ ) from the H1, H2 and H4 segments.

#### MOUNTAIN-FRONT SINUOSITY (*Smf*)

The results of the *Smf* analysis range from 1.05 to 2.02 along the mountain-fronts of the Hoyran Graben (Table 2). While the lowest *Smf* value was obtained from the K2 segment, the highest value was acquired from the H6 segment. Overall, the southern segments show lower *Smf* values than do the northern segments (Fig. 8A, B).

#### VALLEY FLOOR WIDTH-TO-VALLEY HEIGHT INDEX (*Vf*)

In the *Vf* analysis, transverse valley profiles were taken between ~200 and ~250 m (representative assessment of the valley morphology) upstream of the mountain fronts (Fig. 8A, B). The mean *Vf* values range between 0.11 and 1.34 (Table 2). The lowest *Vf* value was obtained from the S1 segment, representing highly incised and V-shaped valleys. The highest value was determined from the H6 segment, corresponding to flat-floored valleys.

#### DRAINAGE BASIN ASYMMETRY (*AF*)

The drainage basin asymmetry factor index was calculated for all sub-basins in the study area and the results were divided into three categories. Symmetrical sub-basins are shown as green two-sided arrows, left-hand side tilting red, and right-hand side tilting blue arrows (Fig. 8A, B). According to the results obtained, the *AF* values are between 13.76 and 87.03 and the sub-basins are mostly asymmetrical (Table 2). The U1, S2 and H3 segments mostly represent westwards tilting ones, while the S2, K3, H5 and H6 segments slope eastwards.

#### STREAM LENGTH GRADIENT INDEX (*SL*)

The *SL* values for streams cutting through the fault segments ranged from 1.48 to 9450 (Fig. 9). The lowest values were obtained for the Hoyran Graben's main drainage region and the upstream reaches of the drainage sub-basins. The

highest values, related to faults rather than to lithological changes, were obtained for the U1, S1, S2, K1, K2 segments and represent streams consistent with the faults' strikes.

#### NORMALIZED CHANNEL STEEPNESS INDEX (*Ksn*)

The *Ksn* values calculated in the Hoyran Graben range between 2.38 and 990.38. The highest values ( $Ksn > 400$ ) are located at the southwestern part of the graben (U1, S1 and S2), while lower values were obtained from its central to northeastern part (Fig. 10).

## DISCUSSION

#### INTERPRETATION OF GEOMORPHIC INDICES AND RELATIVE TECTONIC ACTIVITY ASSESSMENT OF SEGMENTS

The lowest *Smf* values correspond to the U1, K1 and K2 segments, indicating relatively high tectonic activity ( $1.05 < Smf < 1.12$ ). They are followed by the values obtained for the S1, K3, H1, H2, H3 and H4 segments ( $1.20 < Smf < 1.41$ ). A third group have higher values (S2, H5 and H6;  $1.62 < Smf < 2.02$ ) that indicate moderate activity (classes are taken from Özkaymak and Sözbilir, 2012; Özkaymak, 2014).

The *Vf* values calculated for the valleys controlled by the fault segments range between 0.11 and 1.34. The *Vf* and *Smf* values are compatible for the U1, S1, K1, H1 and H4 segments, having V-shaped valley profiles, with the lowest values indicating high tectonic activity ( $Vf < 0.34$ ). The highest *Vf* values correspond to the H5 and H6 segments that are highly eroded, the valleys being flat-floored and reflecting lower tectonic activity (Bull and McFadden, 1977; Keller and Pinter, 2002). The *Vf* values can be correlated with the *Smf* values, which made it possible to estimate the activity class and uplift rate for each segment as suggested by Rockwell et al. (1984; Fig. 11). According to this classification, the U1, S1, K1, K2, K3, H1, H2, H3 and H4 segments show high tectonic activity with an uplift rate of  $> 0.5$  mm/y, while the H5 and H6 segments demonstrate moderate activity and have an uplift rate of 0.05–0.5 mm/y. These uplift rates are compatible with those of the Pliocene rates (0.2–0.3 mm/y) suggested for the Western Anatolian Province (Demir et al., 2004), and with those of the Quaternary rates (0.1–0.2 mm/y) for the Büyük Menderes region (Westaway et al., 2003).

The hypsometric curves of the fault segments indicate that the highest potential for tectonic activity should be expected at the southeastern margin of the Hoyran Graben, in particular in the S2, K1 and K2 segments which show a concave curvature.

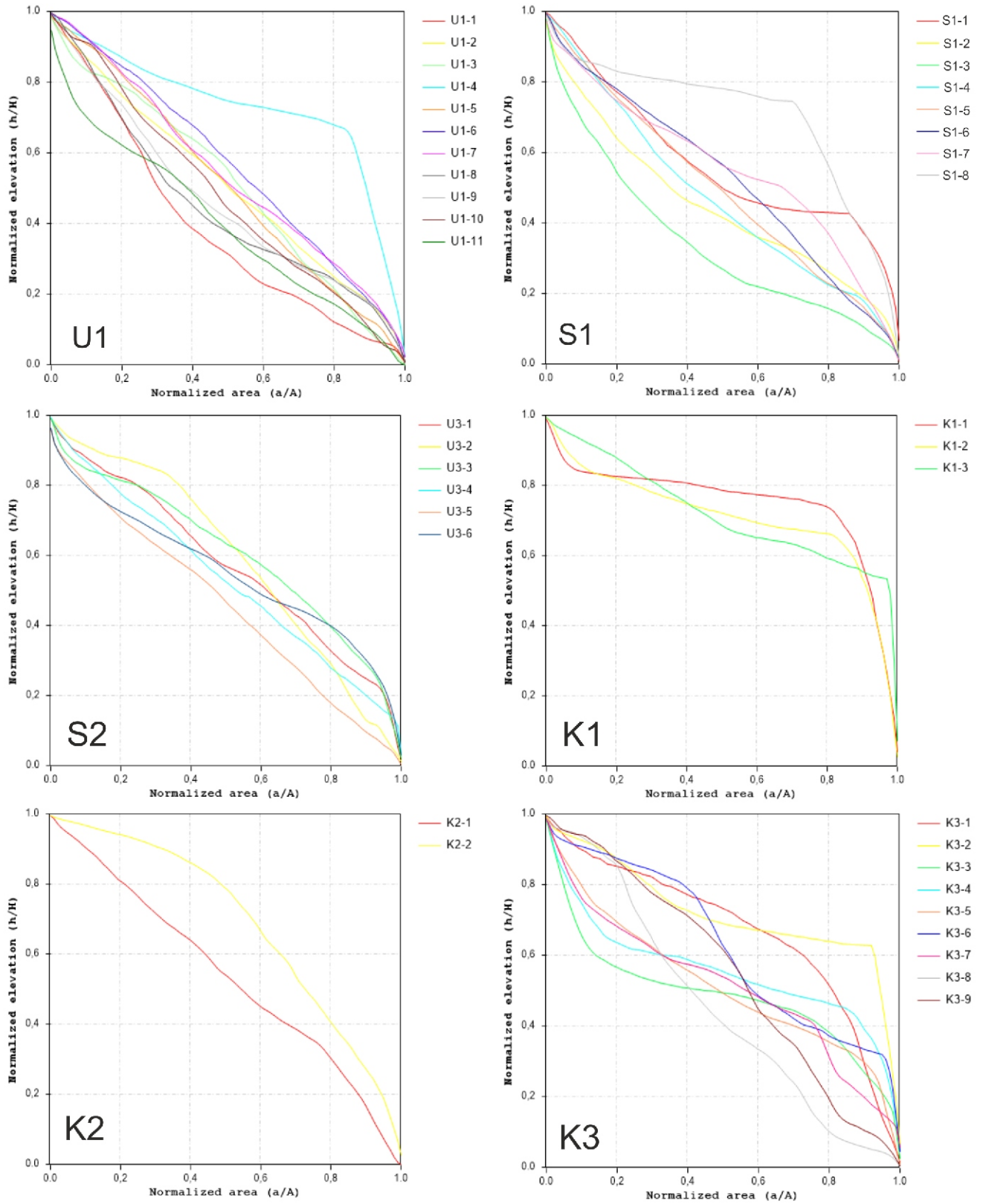


**Fig. 6. Hypsometric curves of the Hoyran Graben's drainage system**

The colour codes for different fault segments are indicated in the legend

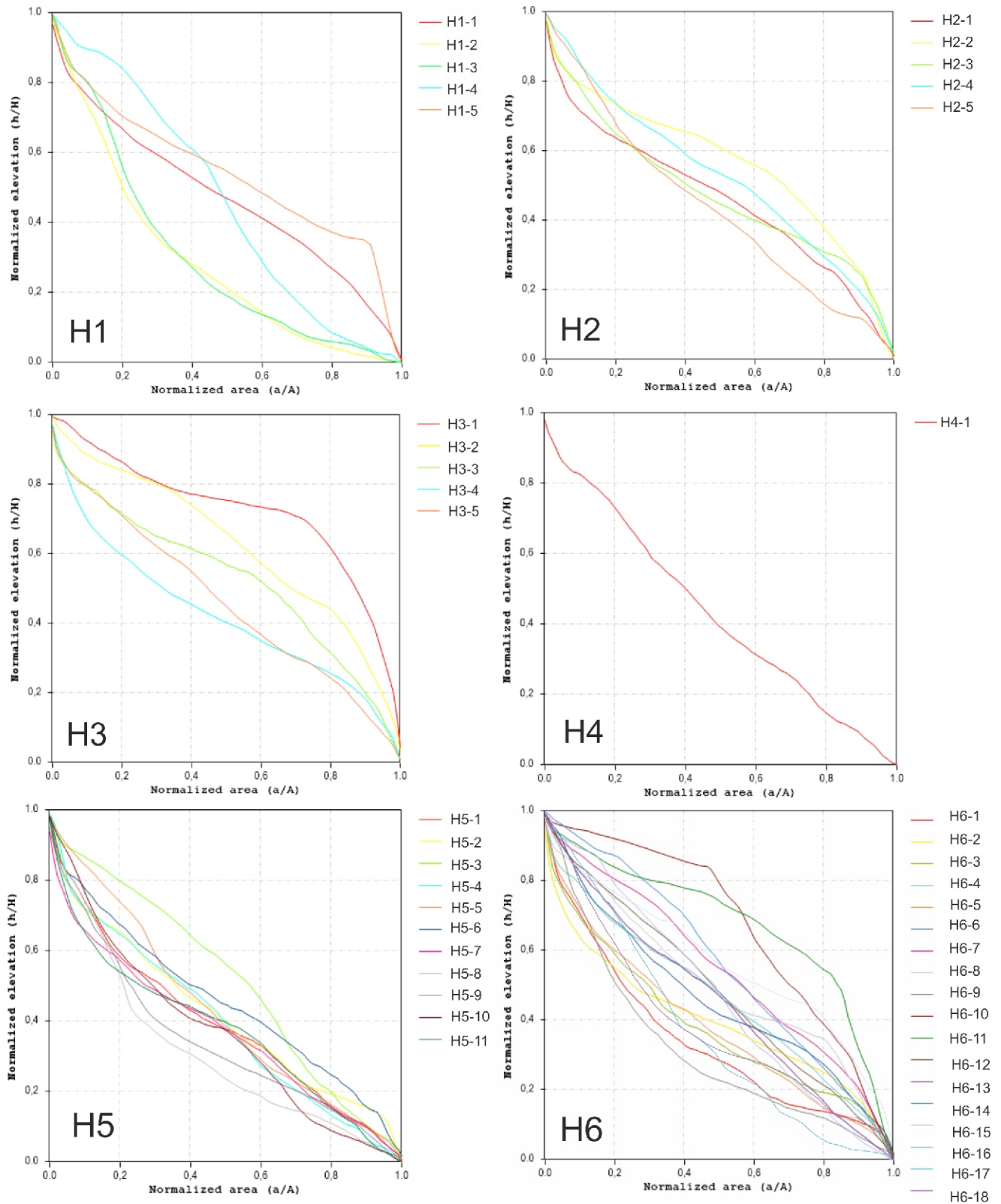


Fig. 6 cont.

Table 2

**Morphological properties of fault segments in the Hoyran Graben showing basin area, drainage basin asymmetry (*AF*), valley floor width-to-valley height ratio (*Vf*), hypsometric integral (*HI*) and mountain-front sinuosity (*Smf*)**

Segment no.	Basin no.	Basin area [km <sup>2</sup> ]	<i>AF</i>	<i>AF</i> (mean)	<i>Vf</i>	<i>Vf</i> (mean)	<i>HI</i>	<i>HI</i> (Mean)	<i>Lmf</i> [km]	<i>Ls</i> [km]	<i>Smf</i>
U1	U1-1	1.38	79.72	63.61	0.31	0.25	0.39	0.51	10.56	9.4	1.12
	U1-2	1.45	36.62		0.18		0.51				
	U1-3	0.99	84.40		1.25		0.51				
	U1-4	7.39	48.59		0.02		0.73				
	U1-5	0.75	66.45		0.12		0.51				
	U1-6	1.00	74.65		0.08		0.57				
	U1-7	1.37	82.62		0.17		0.55				
	U1-8	1.17	65.68		0.39		0.45				
	U1-9	1.36	73.28		0.18		0.46				
	U1-10	2.41	46.52		0.01		0.48				
	U1-11	1.30	41.14		0.02		0.40				
S1	S1-1	8.31	55.63	51.44	0.20	0.11	0.57	0.52	10.54	8.79	1.20
	S1-2	1.16	44.31		0.15		0.45				
	S1-3	3.45	69.12		0.01		0.34				
	S1-4	1.39	33.85		0.15		0.48				
	S1-5	12.40	52.88		0.13		0.50				
	S1-6	1.75	41.11		0.03		0.53				
	S1-7	2.68	44.98		0.20		0.56				
	S1-8	1.63	69.63		0.02		0.71				
S2	S2-1	5.01	74.31	59.07	0.41	0.14	0.58	0.56	15.82	9.79	1.62
	S2-2	0.69	67.35		0.09		0.59				
	S2-3	13.84	62.46		0.05		0.61				
	S2-4	0.83	61.16		0.03		0.53				
	S2-5	0.71	50.83		0.02		0.46				
	S2-6	1.11	38.32		0.25		0.56				
K1	K1-1	0.75	82.40	64.87	0.11	0.29	0.75	0.73	7.32	6.56	1.12
	K1-2	0.74	44.75		0.09		0.71				
	K1-3	0.79	67.47		0.66		0.72				
K2	K2-1	1.79	52.27	57.07	0.14	0.66	0.54	0.62	4.2	4.01	1.05
	K2-2	1.40	61.87		1.18		0.69				
K3	K3-1	1.74	45.16	49.73	0.22	0.81	0.67	0.57	20.76	16.46	1.26
	K3-2	5.22	30.69		0.41		0.72				
	K3-3	18.43	69.94		0.21		0.49				
	K3-4	4.12	21.78		0.32		0.56				
	K3-5	1.73	71.59		0.80		0.52				
	K3-6	8.15	36.27		0.52		0.63				
	K3-7	0.77	42.30		0.25		0.52				
	K3-8	9.83	69.51		0.03		0.46				
	K3-9	1.04	60.36		4.50		0.55				
H1	H1-1	0.98	35.20	53.21	0.02	0.33	0.47	0.41	10.19	7.54	1.35
	H1-2	16.60	19.99		0.12		0.29				
	H1-3	1.04	54.27		0.21		0.30				
	H1-4	1.64	70.96		3.12		0.46				
	H1-5	35.98	85.63		0.75		0.54				
H2	H2-1	1.22	49.28	64.89	0.83	0.70	0.46	0.49	6.18	4.37	1.41
	H2-2	3.10	56.21		0.19		0.56				
	H2-3	4.38	77.71		0.09		0.48				
	H2-4	1.73	74.16		1.97		0.53				
	H2-5	12.66	67.10		0.41		0.44				
H3	H3-1	2.72	54.31	56.83	0.58	0.53	0.72	0.56	7.39	5.75	1.29
	H3-2	8.83	69.35		0.85		0.63				
	H3-3	0.73	65.98		0.12		0.53				
	H3-4	1.95	30.94		0.68		0.43				
	H3-5	1.72	63.55		0.43		0.47				

Tabl. 2 cont.

H4	H4-1	0.71	48.06	48.06	0.34	0.34	0.43	0.43	4.35	3.31	1.31
H5	H5-1	0.62	87.03	41.11	0.73	1.16	0.39	0.4	18.73	11.11	1.69
	H5-2	3.17	20.99		0.18		0.42				
	H5-3	15.91	60.58		0.88		0.52				
	H5-4	6.90	42.06		0.53		0.40				
	H5-5	11.05	13.76		0.90		0.43				
	H5-6	1.17	30.89		4.07		0.46				
	H5-7	9.86	38.09		1.00		0.38				
	H5-8	6.22	47.54		1.30		0.31				
	H5-9	6.56	19.56		0.44		0.35				
	H5-10	1.39	36.81		0.61		0.37				
	H5-11	0.92	54.94		2.16		0.38				
H6	H6-1	1.63	40.64	42.70	0.68	1.34	0.34	0.47	26.22	13.01	2.02
	H6-2	2.57	51.53		0.37		0.40				
	H6-3	0.91	24.97		0.81		0.38				
	H6-4	1.07	53.95		0.94		0.47				
	H6-5	1.57	17.45		1.20		0.39				
	H6-6	5.10	27.58		0.28		0.47				
	H6-7	2.53	35.45		0.51		0.55				
	H6-8	0.76	36.13		0.58		0.50				
	H6-9	6.81	35.23		0.91		0.32				
	H6-10	1.88	30.75		0.60		0.67				
	H6-11	1.98	70.64		0.20		0.68				
	H6-12	14.34	72.99		2.45		0.49				
	H6-13	0.77	52.49		1.79		0.45				
	H6-14	29.66	81.03		0.57		0.56				
	H6-15	0.98	18.90		2.21		0.47				
	H6-16	0.74	41.67		1.83		0.57				
	H6-17	0.76	34.47		7.80		0.37				
	H6-18	43.38	46.16		0.46		0.39				

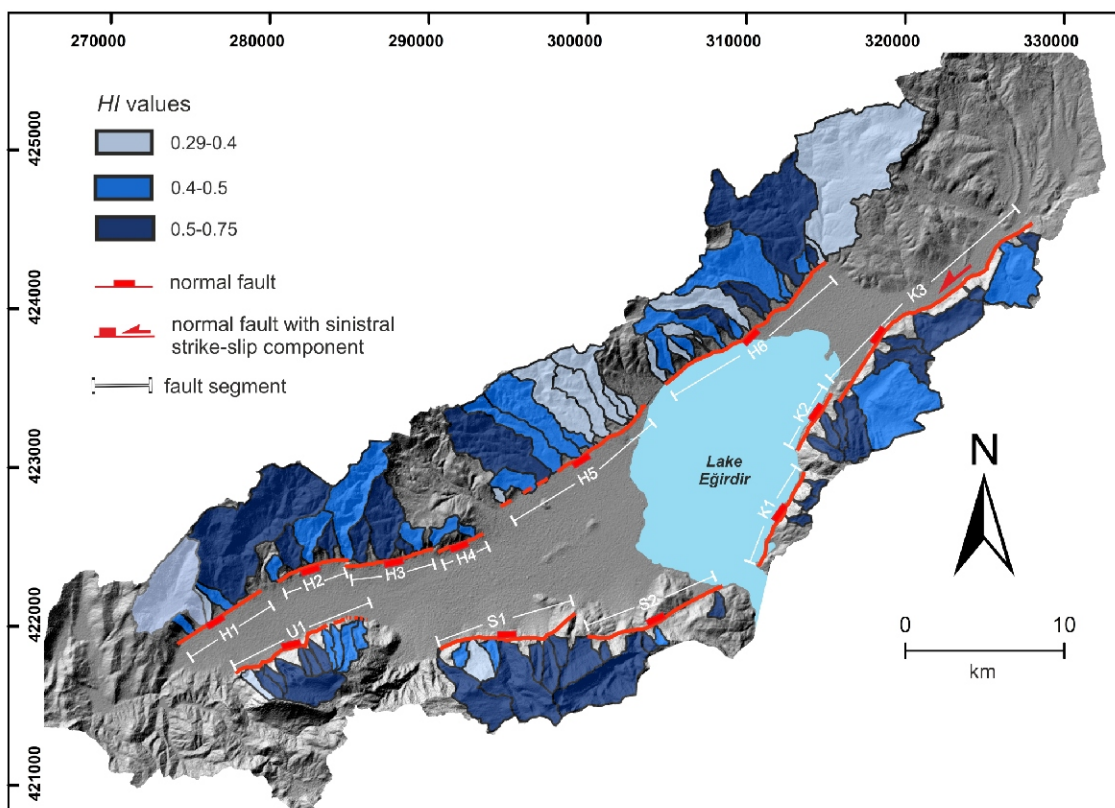


Fig. 7. Map showing the hypsometric integral (HI) values of drainage sub-basins of the Hoyran Graben (see Fig. 4 for the explanation of HI values)

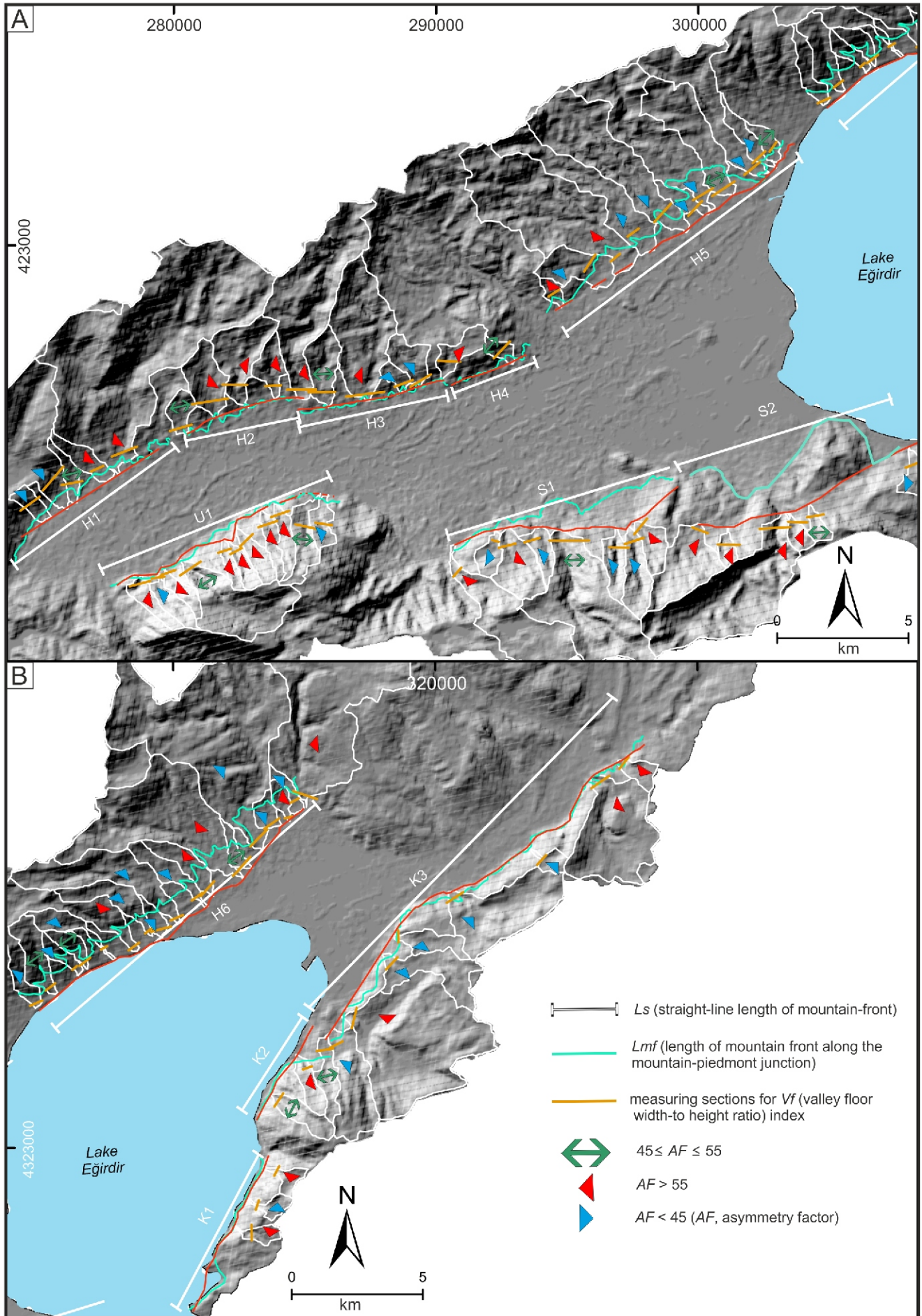


Fig. 8. Schematic watershed map of the Hoyran Graben showing the tilting of the drainage sub-basins controlled by fault segments

A – the western part; B – the eastern part;  $L_{mf}$  and  $L_s$  are the lines used for the calculations of  $S_{mf}$  in the study area

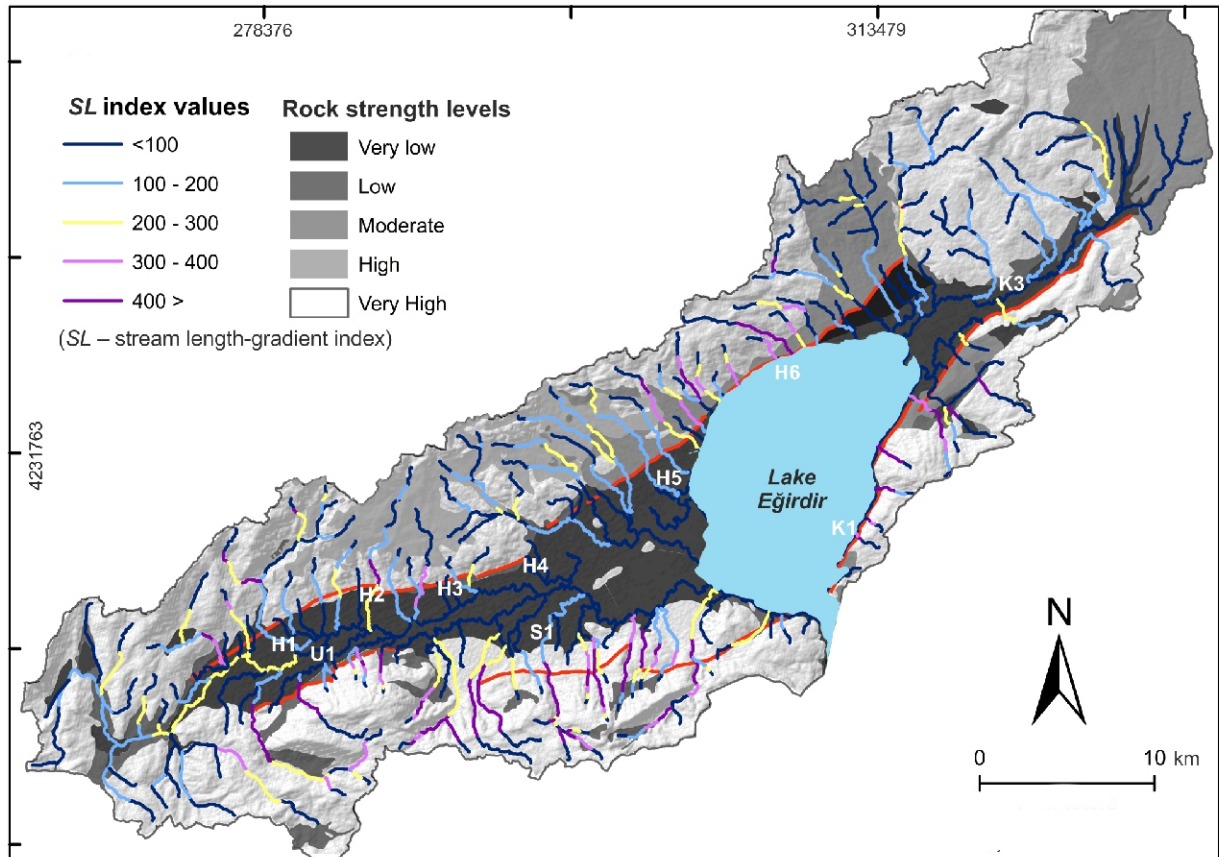


Fig. 9. Simplified map showing the SL values along the drainage of the Hoyran Graben where the rock strength classification (Selby, 1980) is shown on a geological map of the study area

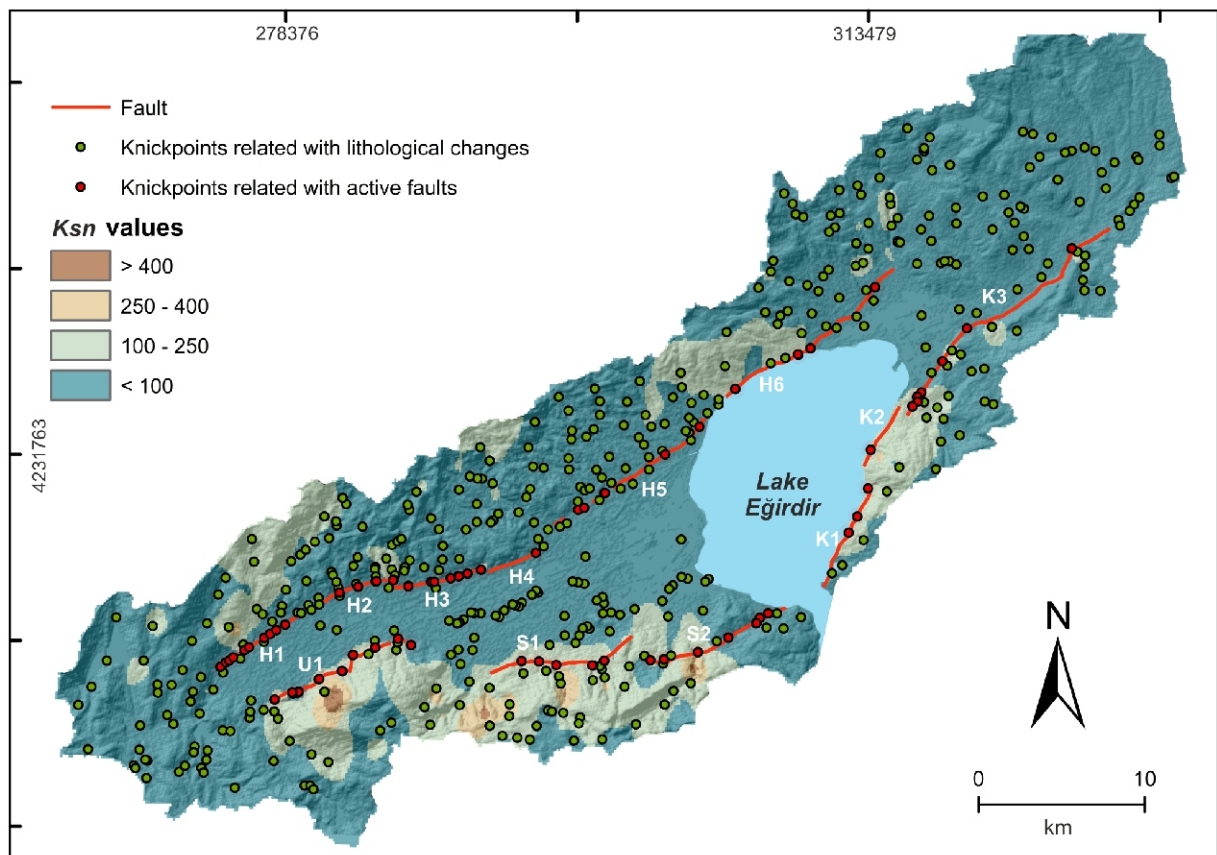
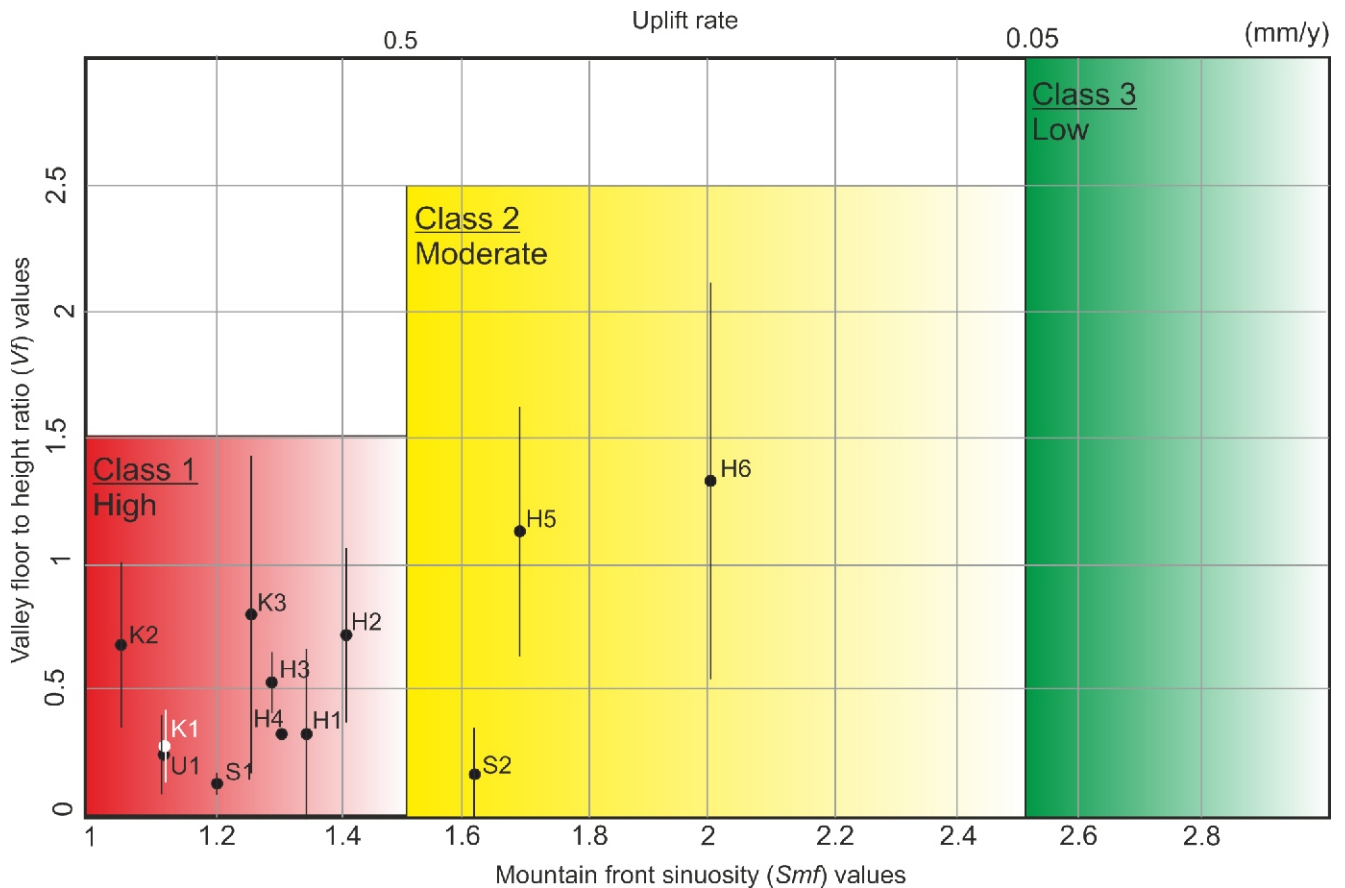


Fig. 10. Map showing the knickpoint distribution, related to lithological changes and active faulting, and sensitivity of the normalized channel steepness index (Ksn) of the study area to active tectonism in the Hoyran Graben



**Fig. 11. Chart showing the  $Smf$  (mountain-front sinuosity) versus  $Vf$  (ratio of valley floor width-to-valley height index) values (vertical bars show standard deviations for  $Vf$  values) for the mountain fronts of the Hoyran Graben and inferred activity classes (Silva et al., 2003) where the upper x-axis indicates inferred uplift rates (mm/y) (from Rockwell et al., 1984; Yıldırım, 2014)**

They are followed by the U1 and H3 segments showing slight concavity. The remaining segments mostly indicate a linear and/or convex curvature, corresponding to lower tectonic activity or stable conditions. The  $HI$  calculations mostly support the  $HC$ ,  $Smf$  and  $Vf$  results, with some differences that suggest relatively higher activity for the U1, S1, S2, K1, K2, K3 and H3 segments ( $HI > 0.5$ ). These values are compatible with those calculated for the Spiladağı ( $HI > 0.61$ ) (Özkaymak and Sözbilir, 2012), the Honaz Fault ( $0.61 < HI < 0.73$ ) (Özkaymak, 2014) and the Çameli Basin ( $0.31 < HI < 1.05$ ) (Özsayın, 2016) located in the western part of the study area.

According to the results of drainage basin asymmetry obtained, the  $AF$  values are between 13.76 and 87.03. For the U1, S2 and H3 segments, the sub-basins tilt mostly westwards, suggesting higher tectonic activity. On the other hand, for the K1, K2 and K3 segments of the southeastern margin, the asymmetry of sub-basins does not represent uniform tilting. This situation may be a consequence of lower tectonic activity and/or the existence of the lake and related depositional processes. The existence of the lake, creating a local base level for a drainage system, may have reduced the incision of the river profile. This situation may also increase sedimentation and affect basin geometry. At the northwestern margin, tilting of the sub-basins show that the central part of the H1 segment matches the behaviour of normal faults as indicated by Faulds and Varga (1998). Tilting along the H2 segment also suggests the activity of the H1 segment as most of the sub-basins tilt to the west. The H3 and H4 segments do not represent a uniform pattern, while the H5 and H6 ones show eastwards tilting. This asymmetry

may suggest high activity along the northern margin of the Lake Eğirdir, but morphometric analysis does not indicate higher activity for this section. This might be a consequence of lithological differences, as the footwalls of the H5 and H6 segments are composed of Miocene lacustrine deposits, which are less resistant to erosion than are basement units.

The  $SL$  values also support the results of other geomorphic indices. Higher  $SL$  values were obtained from the U1, S1, S2, K1 and K2 segments. They suggest higher activity at the southeastern margin of the Hoyran Graben. In this section, the slope-breaks are mostly related to tectonic activity, indicating rock strength changes due to the juxtaposition of the basement units with Quaternary deposits along the fault segments. By contrast, at the northwestern margin, the  $SL$  values mostly change due to lithological differences rather than to fault activity, with the exception of the H2 and H3 segments. Thus, the uphill increase of the  $SL$  values is not as high as at the southern margin of the Hoyran Graben and cannot be directly associated with fault activity.

The  $Ksn$  values indicate three major areas that have the highest values. These are located at the southern parts of the U1, S1, S2 and K2 segments. Relatively higher  $Ksn$  values were also obtained at the northern part of the H1 segment. Due to higher  $Ksn$  values, it can be suggested that the fault segments which control the southwestern part of the Hoyran Graben represent higher tectonic activity. Nevertheless, the lower values located at the northeastern part are thought to have been generated from lithological changes, where the basement units are unconformably overlain by the basin infill.



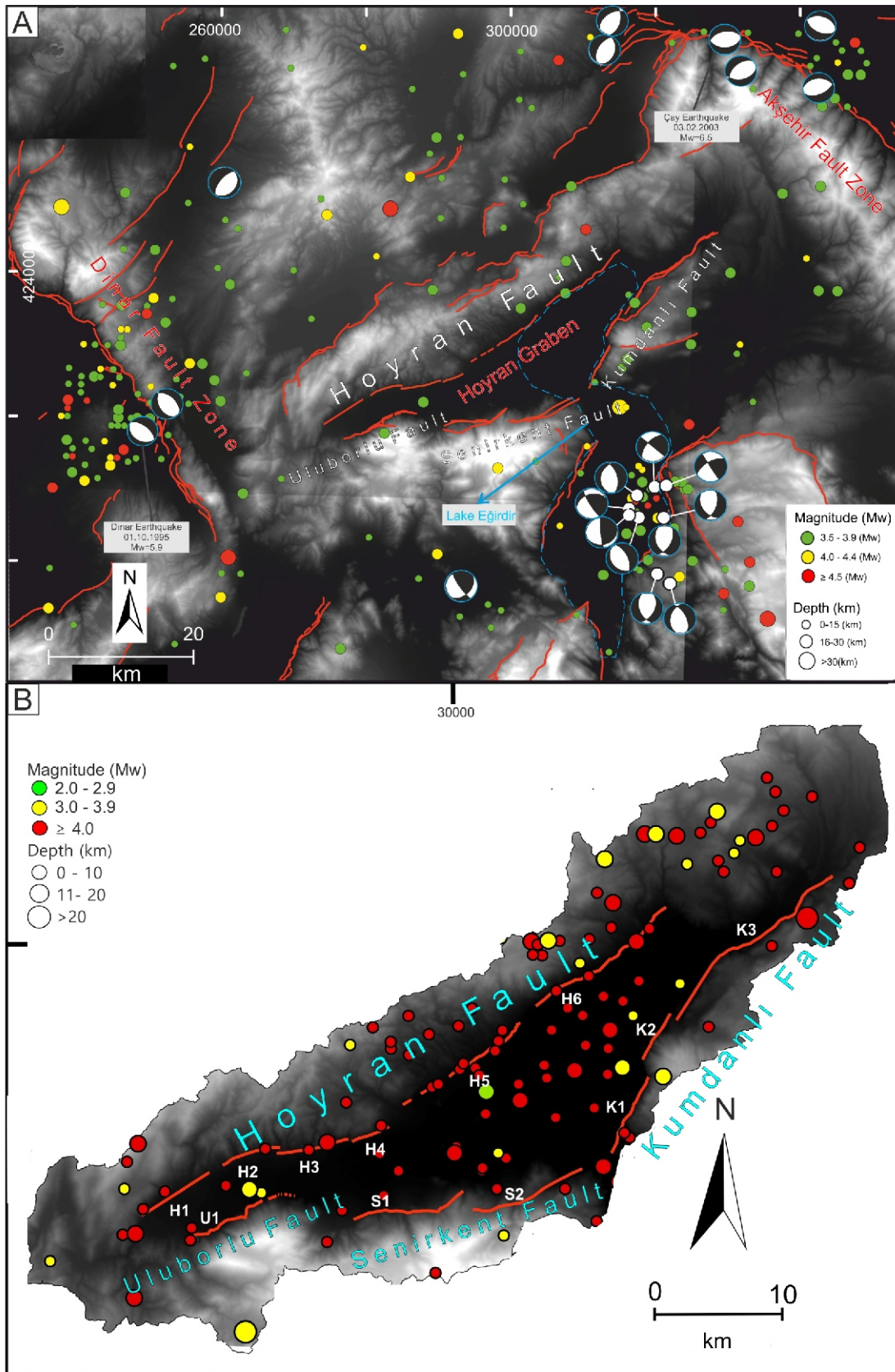


Fig. 12. Digital elevation model of the Hoyran Graben and surrounding region showing the epicentres of earthquakes

A – with magnitude Mw 3.5 which occurred in the northwestern part of the Isparta Bend between 1901 and 2023; B – with magnitudes M 2.0 which occurred in the Hoyran Graben between 1901 and 2023 (KOERI, 2023); active faults are taken from Emre et al. (2013)

To summarize, the results of geomorphic indices clearly show that the highest relative tectonic activity should be expected from the U1, S1, S2, K1 and H1 segments. Moderate activity is indicated in the K2, K3, H2, H3 and H4 segments, while relatively lower activity should be expected from the H5 and H6 segments. The highest relative activity is calculated for the southwestern part of the Hoyran Graben.

The difference in activity is related to the location of the graben. According to the GPS data, both flanks of the Isparta Bend are moving to the west, and the western one is faster than the eastern (Reilinger et al., 1997; McClusky et al., 2000). This velocity variance is suggested to cause higher tectonic activity in the southwestern part of the Hoyran Graben.

#### INTERPRETATION OF SEISMIC ACTIVITY IN THE HOYRAN GRABEN

The northwestern part of the Isparta Bend is one of the most seismically active regions in Anatolia. This area is characterised by several seismically active faults, having different orientations. Significant earthquakes occurred in 1995 (Dinar: Mw 5.9) and 2002 (Çay: Mw 6.5). The earthquake distribution is concentrated in three regions around the study area (Fig. 12A). These are the Akşehir Fault Zone, Dinar Fault Zone and the Lake Eğirdir region. The NW-trending Akşehir Fault Zone is composed of several segments that show normal fault characteristics (Koçyiğit and Özacar, 2003; Emre et al., 2003; Akyüz et al., 2006). The epicentre of the 2002 Çay earthquake was located at the western end of this zone. The focal mechanism solutions of earthquakes clustered in this area reflect approximately E–W oriented extension. Some of the solutions which represent nearly N–S extension may be related to stress variation as the region is located at the hinge zone of the Isparta Bend.

The second cluster relates to the Dinar Fault Zone, where the Dinar earthquake took place in 1995. This fault zone is also characterised by NW-trending normal faults, compatible with the focal mechanism solution of the Dinar earthquake (Altunel et al., 1999; Özalp et al., 2018; Kürçer et al., 2021). The third cluster corresponds to the Lake Eğirdir region with NNE-trending normal faults. The focal mechanism solutions of earthquakes, clustered in this area, indicate approximately E–W-oriented extension. Some of the solutions which show strike-slip dominated faulting can be generated by transfer faults, bounding the stepover zones of NNE-trending normal faults (Faulds and Varga, 1998).

Within the stress distribution, the palaeostress analysis results obtained for the U1, H2 and K3 segments of the Hoyran Graben mostly fit with those recorded in the Lake Eğirdir region. The seismicity in the graben is typically clustered along the Uluborlu, Kumdanlı and eastern part of the Hoyran faults (central part of Lake Eğirdir). The distribution of the earthquake epicentres partially overlaps with the results of the morphometric analysis, as they indicate lower tectonic activity for the H5 and H6 segments. The eastern part of the Hoyran Graben constitutes the lowest elevation of the depression, where most of the epicentres are located. This situation may be the result of buried faulting and/or relatively high seismic activity along the H5 and H6 segments.

Additionally, the result of the palaeoseismological studies of the Kumdanlı Fault show traces of earthquakes that formed a surface rupture during the Late Pleistocene–Holocene interval (Özalp et al., 2017). In this case, the possibility of buried faults should be taken into consideration, as no destructive earthquakes have been recorded along the Hoyran Graben faults. However, the low-magnitude earthquake epicentres docu-

mented during the instrumental survey period indicate that these faults are still seismically active (Fig. 12B). Moreover, the faults forming the Hoyran Graben, located at the centre of three seismically active zones (Lake Eğirdir, Akşehir and Dinar), have a significant earthquake risk potential, which can be considered as a seismic gap.

Furthermore, previous studies have outlined the development of the Hoyran Graben as a N–S-oriented depression, resulting from contraction between the African and Eurasian plates (e.g., Karaman, 2010; Faccenna et al., 2014; Van Hinsbergen et al., 2020). Subsequently, it was proposed that the current morphology of this depression is a result of its intersection with the Fethiye-Burdur Fault Zone and simultaneous counter-clockwise rotation. However, seismic analyses of three active regions surrounding the study area reveal no evidence of strike-slip faulting. This observation raises the possibility that the Fethiye-Burdur Fault Zone, which likely influenced the formation of the Hoyran Graben and adjacent depression areas, may currently be inactive or that its fault planes exhibit reactivation with dissimilar characteristics.

#### CONCLUSIONS

In this study, the faults bounding the Hoyran Graben in Western Anatolia were evaluated in the light of field observations and geomorphic indices and the following results were obtained.

1. The Hoyran Graben, trending approximately NE, is delineated by the Hoyran, Uluborlu, Senirkent and Kumdanlı faults, representing seismic activity.
2. The Hoyran Fault, establishing the northern limit of the graben, comprises six segments, while the Uluborlu Fault, forming its southern boundary, consists of one segment; the Senirkent Fault has two segments, and the Kumdanlı Fault comprises three segments.
3. The morphology formed by the boundary faults of the Hoyran Graben was evaluated quantitatively through 7 geomorphic indices. The Uluborlu Fault (U1), Senirkent Fault (S1-S2), and Kumdanlı Fault (K1) segments, constituting the southern border, along with the Hoyran Fault (H1) segment at the southwest terminus, exhibit the highest levels of tectonic activity. Calculations indicate that the southwest side of the Hoyran Graben experiences more rapid deformation ( $> 0.5$  mm/y) compared to the northeast (0.05–0.5 mm/y).
4. The variation in deformation rates on opposing sides of the Hoyran Graben is attributed to the swifter westwards movement of the western flank of the Isparta Bend on the outer part of the wing compared to the inner side.
5. The Fethiye-Burdur Fault Zone probably has significant importance in shaping the geometry of depressions such as the Hoyran Graben. Nevertheless, contemporary projections suggest that the fault planes within this zone are either inactive or exhibit reactivation with different characteristics.
6. Positioned within a seismically active region, the Hoyran Graben has experienced earthquakes in neighbouring fault zones. The absence of destructive earthquakes during the period of instrumental surveys along the graben is considered a noteworthy gap in terms of seismic activity.

**Acknowledgements.** This work was supported by the Scientific Research Coordination Unit of Hacettepe University (Project no FHD-2021-19432). The authors are grateful to three anonymous reviewers for their valuable comments and suggestions to improve this manuscript.

## REFERENCES

- Agostini, S., Doglioni, C., Innocenti, F., Manetti, P., Tonarini, S., 2010. On the geodynamics of the Aegean rift. *Tectonophysics*, 488: 7–21; <https://doi.org/10.1016/j.tecto.2009.07.025>
- Aktuğ, B., Nocquet, J.M., Cingöz, A., Parsons, B., Erkan, Y., England, P., Lenk, O., Gürdal, M.A., Kılıçoğlu, A., Akdeniz, H., Tekgül, A., 2009. Deformation of western Turkey from a combination of permanent and campaign GPS data: limits to block-like behaviour. *Journal of Geophysical Research*, 114: 1–22; <https://doi.org/10.1029/2008JB006000>
- Akyüz, H.S., Uçarkuş, G., Şatır, D., Dikbaş, A., Kozacı, Ö., 2006. Paleoseismological investigations on surface rupture from the 3 February 2002 Çay earthquake (in Turkish with English summary). *Bulletin for Earth Sciences*, 27: 41–52.
- Alçiçek, M.C., 2015. Comment on “The Fethiye–Burdur fault zone: a component of upper plate extension of the subduction transform edge propagator fault linking hellenic and cyprus arcs, eastern mediterranean. *Tectonophysics*, 635, 80–99” by J. Hall, A.E. Aksu, İ. Elitez, C. Yalıtırak, G. Çiftçi. *Tectonophysics*, 664: 5–13; <https://doi.org/10.1016/j.tecto.2015.01.025>
- Alipoor, R., Poorkermani, M., Zare, M., El Hamdouni, R., 2011. Active tectonic assessment around Rudbar Lorestan dam site, high Zagros belt (SW of Iran). *Geomorphology*, 128: 1–14; <https://doi.org/10.1016/j.geomorph.2010.10.014>
- Altunel, E., Barka, A., Akyüz, S., 1999. Palaeoseismicity of the Dinar Fault, SW Turkey. *Terra Nova*, 11: 297–302; <https://doi.org/10.1046/j.1365-3121.1999.00262.x>
- Ambraseys, N.N., 1988. Engineering seismology. *Journal of Earthquake Engineering and Structural Dynamics*, 17: 1–105; <https://doi.org/10.1002/eqe.4290170102>
- Ambraseys, N.N., Jackson, J.A., 1998. Faulting associated with historical and recent earthquakes in the Eastern Mediterranean region. *Geophysical Journal International*, 133: 390–406; <https://doi.org/10.1046/j.1365-246X.1998.00508.x>
- Azañón, J.M., Galve, J.P., Pérez-Peña, J.V., Giaconia, F., Carvajal, R., Booth-Rea, G., Roldán, F.J., 2015. Relief and drainage evolution during the exhumation of the Sierra Nevada (SE Spain): Is denudation keeping pace with uplift? *Tectonophysics*, 663: 19–32; <https://doi.org/10.1016/j.tecto.2015.06.015>
- Balci, V., 2011a. 1/100,000 scale Geological Maps of Turkey. General Directorate of Mineral Research And Exploration, Afyon L-24 Sheet (No: 162).
- Balci, V., 2011b. 1/100,000 scale Geological Maps of Turkey. General Directorate of Mineral Research and Exploration, Afyon L-25 Sheet (No: 161).
- Barka, A., Reilinger, R., Şaroğlu, F., Şengör, A.M.C., 1995. The Isparta Angle: its evolution and importance in the tectonics of the eastern Mediterranean region. *International Earth Sciences Colloquium on the Aegean Region, Proceedings*: 3–17.
- Barka, A., Reilinger, R., 1997. Active tectonics of the Eastern Mediterranean region: deduced from GPS, neotectonic and seismicity data. *Annals of Geophysics*, 40: 587–610; <https://doi.org/10.4401/ag-3892>
- Bellin, N., Vanacker, V., Kubik, P.W., 2014. Denudation rates and tectonic geomorphology of the Spanish Betic Cordillera. *Earth and Planetary Science Letters*, 390: 19–30; <https://doi.org/10.1016/j.epsl.2013.12.045>
- Biddle, K.T., Christie-Blick, N., 1985. Glossary strike-slip deformation, basin formation, and sedimentation. *Society of Economic Mineralogists Special Publication*, 37: 375–386; <https://doi.org/10.2110/pec.85.37.0001>
- Bishop, P., Hoey, T.B., Jansen, J.D., Artza, I.L., 2005. Knickpoint recession rate and catchment area: the case of uplifted rivers in Eastern Scotland. *Earth Surface Processes and Landforms*, 30: 767–778.
- Blumenthal, M.M., 1947. Geology of the Taurus at the hinterland of Seydişehir-Beyşehir (in Turkish with English summary). General Directorate of Mineral Research and Exploration publications, Serie D, 2.
- Blumenthal, M.M., 1951. Recherches géologiques dans le Taurus occidental dans l'arrière-pays d'Alanya. General Directorate of Mineral Research and Exploration publications, Serie D, 5.
- Bozkurt, E., 2001. Neotectonics of Turkey – a synthesis. *Geodinamica Acta*, 14: 3–30; <https://doi.org/10.1080/09853111.2001.11432432>
- Bozkurt, E., Park, R.G., 1994. Southern Menderes Massif an incipient metamorphic core complex in western Anatolia, Turkey. *Journal of the Geological Society*, 151: 213–216; <https://doi.org/10.1144/gsjgs.151.2.0213>
- Bozkurt, E., Rojay, B., 2005. Plio-Quaternary evolution of the Küçük Menderes Graben Southwestern Anatolia, Turkey. *Geodinamica Acta*, 18: 299–316; <https://doi.org/10.3166/ga.18.317-331>
- Brun, J.P., Sokoutis, D., 2010. 45 m.y. of Aegean crust and mantle flow driven by trench retreat. *Geology*, 38: 815–818; <https://doi.org/10.1130/G30950.1>
- Bull, W.B., 1977. Tectonic geomorphology of the Mojave Desert, California. US Geological Survey Contract Report 14-0-001-G394. Office of Earthquakes, Volcanoes, and Engineering, Menlo Park, California.
- Bull, W.B., McFadden, L.D., 1977. Tectonic geomorphology north and south of the Garlock fault, California. In: *Geomorphology in arid regions* (ed. D.O. Doehring): 115–138. *Proceedings at the Eighth Annual Geomorphology Symposium*, State University of New York, Binghamton, NY.
- Burbank, D.W., Anderson, R.S., 2013. *Tectonic Geomorphology*. Oxford, Blackwell Science, 2nd edition.
- Camafort, M., Pérez-Peña, J.V., Booth-Rea, G., Melki, F., Gracia, E., Azañón, J.M., Galve, J.P., Marzougui, W., Gaidi, S., Ranero, C., 2020. Active tectonics and drainage evolution in the Tunisian Atlas driven by interaction between crustal shortening and mantle dynamics. *Geomorphology*, 351: 106954; <https://doi.org/10.1016/j.geomorph.2019.106954>
- Delvaux, D., Sperner, B., 2003. Stress tensor inversion from fault kinematic indicators and focal mechanism data: the TENSOR program. *Geological Society Special Publications*, 212: 75–100; <https://doi.org/10.1144/GSL.SP.2003.212.01.06>
- Delvaux, D., Moeys, R., Stapel, G., Petit, C., Levi, K., Miroshnichenko, A., Ruzhich, V., Sankov, V., 1997. Paleostress reconstructions and geodynamics of the Baikal region, Central Asia, Part 2. Cenozoic rifting. *Tectonophysics*, 282: 1–38; [https://doi.org/10.1016/S0040-1951\(97\)00210-2](https://doi.org/10.1016/S0040-1951(97)00210-2)
- Demir, T., Yeşilnacar, İ., Westaway, R., 2004. River terrace sequences in Turkey: Sources of evidence for lateral variations in regional uplift. *Proceedings of the Geologists' Association*, 115: 289–311; [https://doi.org/10.1016/S0016-7878\(04\)80010-5](https://doi.org/10.1016/S0016-7878(04)80010-5)
- Dewey, J.F., 1988. Extensional collapse of orogens. *Tectonics*, 6: 1123–1139; <https://doi.org/10.1029/TC007i006p01123>
- Doglioni, C., Agostini, S., Crespi, M., Innocenti, F., Manetti, P., Riguzzi, F., Savasçın, Y., 2002. On the extension in western Anatolia and the Aegean Sea. *Journal of the Virtual Explorer*, 7: 117–131.
- Doğru, A., Görgün, E., Özener, H., Aktuğ, B., 2014. Geodetic and seismological investigation of crustal deformation near İzmir (Western Anatolia). *Journal of Asian Earth Sciences*, 82: 21–31; <https://doi.org/10.1016/j.jseaes.2013.12.008>
- Dumont, J., 1976. La courbure d'Isparta et l'origine des Nappes d'Antalya; hypothese d'un décrochement majeur, l'accident trans-taurique, qui a dedouble le dispositif structural taurique etabli par la tectogenese du cretace superieur. *Bulletin of the Mineral Research and Exploration*, 86: 56–67.
- El Hamdouni, R., Irigaray, C., Fernandez, T., Chacün, J., Keller, E.A., 2008. Assessment of relative active tectonics, southwest border of Sierra Nevada (Southern Spain). *Geomorphology*, 96: 150–173; <https://doi.org/10.1016/j.geomorph.2007.08.004>
- Elitez, İ., Yalıtırak, C., 2014. Miocene-quaternary geodynamics of Çameli Basin, Burdur–Fethiye shear zone (SW Turkey). *Geological Bulletin of Turkey*, 57: 41–67.

- Emre, Ö., Duman, T.Y., Doğan, A., Özalp, S., Tokay, F., Kuşçu, İ., 2003. Surface faulting associated with the Sultandağı earthquake (Mw 6.5) of 3 February 2002, Southwestern Turkey. *Seismological Research Letters*, **74**: 382–392.
- Emre, Ö., Duman, T.Y., Özalp, S., Elmacı, H., Olgun, Ş., Şaroğlu, F., 2013. Active Fault Map of Turkey with Explanatory Text (in Turkish). General Directorate of Mineral Research and Exploration, Special Publication Series-30, Ankara-Türkiye.
- Eyidoğan, H., 1988. Rates of crustal deformation in western Turkey as deduced from major earthquakes. *Tectonophysics*, **148**: 83–92; [https://doi.org/10.1016/0040-1951\(88\)90162-X](https://doi.org/10.1016/0040-1951(88)90162-X)
- Eyidoğan H., Jackson J.A., 1985. A seismological study of normal faulting in the Demirci, Alaşehir and earthquake of 1969–1970 in western Turkey: implications for the nature and geometry of deformation in continental crust. *Geophysical Journal of the Royal Astronomical Society*, **81**: 569–607; <https://doi.org/10.1111/j.1365-246X.1985.tb06423.x>
- Faccenna, C., Becker, T.W., Auer, L., Billi, A., Boschi, L., Brun, J.P., Capitanio, F.A., Funicello, F., Horvath, F., Jolivet, L., 2014. Mantle dynamics in the Mediterranean. *Reviews of Geophysics*, **52**: 283–332.
- Faulds, J.E., Varga, R.J., 1998. The role of accommodation zones and transfer zones in the regional segmentation of extended terranes. *GSA Special Papers*, **323**: 1–45; <https://doi.org/10.1130/0-8137-2323-X.1>
- Ferrater, M., Booth-Rea, G., Pérez-Peña, J.V., Azañón, J.M., Giacomia, F., Masana, E., 2015. From extension to transpression: quaternary reorganization of an extensional related drainage network by the Alhama de Murcia strike-slip fault (eastern Betics). *Tectonophysics*, **663**: 33–47; <https://doi.org/10.1016/j.tecto.2015.06.011>
- Flint, J.J., 1974. Stream gradient as a function of order, magnitude, and discharge. *Water Resources Research*, **10**: 969–973.
- Giacomia, F., Booth-Rea, G., Martínez-Martínez, J.M., Azañón, J.M., Pérez-Peña, J.V., 2012. Geomorphic analysis of the Sierra Cabrera, an active pop-up in the constrictional domain of conjugate strike-slip faults: The Palomares and Polopos fault zones (eastern Betics, SE Spain). *Tectonophysics*, **580**: 27–42. <https://doi.org/10.1016/j.tecto.2012.08.028>
- Görür, N., Şengör, A.M.C., Sakıncı, M., Tüysüz, O., Akkök, R., Yiğitbaş, E., Oktay, F.E., Barka, A.A., Sarıca, N., Ecevitöğlu, B., Demirbağ, E., Ersoy, Ş., Algan, O., Güneysu, C., Akyol, A., 1995. Rift formation in the Gökova region, southwest Anatolia: implications for the opening of the Aegean Sea. *Geological Magazine*, **132**: 637–650; <https://doi.org/10.1017/s0016756800018884>
- Gürer, Ö.F., Sangu, E., Özbüran, M., Gürbüz, A., Sarıca-Filoreau, N., 2013. Complex basin evolution in the Gökova Gulf region: implications on the Late Cenozoic tectonics of southwest Turkey. *International Journal of Earth Sciences*, **102**: 2199–2221; <https://doi.org/10.1007/s00531-013-0909-1>
- Hack, J.T., 1957. Studies of longitudinal profiles in Virginia and Maryland. U.S. Geological Survey, United States Government Printing Office, Washington, Professional Paper 294-B, 1.
- Hack, J.T., 1973. Stream-profile analysis and stream-gradient index. *Journal of Research of the U.S. Geological Survey*, **1**: 421–429.
- Hare, P.W., Gardner, T.W., 1985. Geomorphic Indicators of Vertical Neotectonism along Converging Plate Margins, Nicoya Peninsula, Costa Rica. In: *Tectonic Geomorphology* (eds. M. Morisawa and J.T. Hack): 123–134. Proceedings of the 15th Annual Binghamton Geomorphology Symposium, Allen and Unwin, Boston.
- He, C., Cheng, Y., Rao, G., Chen, P., Hu, J., Yu, Y., Yao, Q., 2018. Geomorphological signatures of the evolution of active normal faults along the Langshan Mountains, North China. *Geodinamica Acta*, **30**: 163–182; <https://doi.org/10.1080/09853111.2018.1458935>
- Hetzl, R., Passchier, C.W., Ring, U., Dora, O.Ö., 1995. Bivergent extension in orogenic belts: the Menderes massif (southwestern Turkey). *Geology*, **23**: 455–458; [https://doi.org/10.1130/0091-7613\(1995\)023<0455:BEIOBT>2.3.CO;2](https://doi.org/10.1130/0091-7613(1995)023<0455:BEIOBT>2.3.CO;2)
- Jackson, J.A., McKenzie, D.P., 1984. Active tectonics of Alpine-Himalayan Belt between western Turkey and Pakistan. *Geophysical Journal of the Royal Astronomical Society*, **77**: 185–265; <https://doi.org/10.1111/j.1365-246X.1984.tb01931.x>
- Jackson J.A., McKenzie D.P., 1988. Rates of active deformation in the Aegean Sea and surrounding regions. *Basin Research*, **1**: 121–128; <https://doi.org/10.1111/j.1365-2117.1988.tb00009.x>
- Jackson, J.A., King, G., Vita-Finzi, C., 1992. The neotectonics of the Aegean: an alternative view. *Earth and Planetary Science Letters*, **61**: 303–318; [https://doi.org/10.1016/0012-821X\(82\)90062-0](https://doi.org/10.1016/0012-821X(82)90062-0)
- Jolivet, L., Brun J.P., 2010. Cenozoic geodynamic evolution of the Aegean. *International Journal of Earth Sciences*, **99**: 109–138; <https://doi.org/10.1007/s00531-008-0366-4>
- Jolivet, L., Faccenna, C., Goffe, B., Mattei, M., Rosetti, F., Brunet, C., Storti, F., Funicello, R., Cadet, J.P., D'Agostino, N., Parra, T., 1998. Midcrustal shear zones in post-orogenic extension: example from the northern Tyrrhenian Sea. *Journal of Geophysical Research*, **103**: 12123–12160; <https://doi.org/10.1016/j.tecto.2012.06.011>
- Jolivet, L., Faccenna, C., Huet, B., Labrousse, L., Pourhiet, L.L., Lacombe, O., Lecomte, E., Burov, E., Dençle, Y., Brun, J.P., Philippon, M., Paul, A., Salaün, G., Karabulut, H., Piromallo, C., Monié, P., Gueydan, F., Okay, A.I., Oberhänsli, R., Pourteau, A., Augier, R., Gadenne, L., Driussi, O., 2013. Aegean tectonics: Strain localisation, slab tearing and trench retreat. *Tectonophysics*, **597–598**: 1–33; <https://doi.org/10.1016/j.tecto.2012.06.011>
- Kahle, H.G., Straub, C., Reilinger, R., McClusky, S., King, R., Hurst, K., Cross, P., 1998. The strain rate field in the Eastern Mediterranean region, estimated by repeated GPS measurements. *Tectonophysics*, **294**: 237–252; [https://doi.org/10.1016/S0040-1951\(98\)00102-4](https://doi.org/10.1016/S0040-1951(98)00102-4)
- Karaman, M.E., 1988. Burdur-Hoyran Fault. 42. Geological Congress, 1-2, Ankara (in Turkish with English summary).
- Karaman, M.E., 1989. Structural evolution of Eğirdir, Kovada, Kaşıkara and Burdur Late Cenozoic basins and their economic potential (in Turkish with English summary). *Türkiye Jeomorfoloji Bülteni*, **17**: 63–70.
- Karaman, M.E., 2010. The tectonic evolution of Lake Eğirdir, West Turkey. *Geologos*, **16**: 223–234.
- Karaoğlu, Ö., Helvacı, C., 2014. Isotopic evidence for a transition from subduction to slab tear related volcanism in western Anatolia, Turkey. *Lithos*, **192–195**: 226–239; <https://doi.org/10.1016/j.lithos.2014.02.006>
- Kaya, O., Ünay, E., Saraç, G., Eichhorn, S., Hassenrück, S., Knappe, A., Pekdeğer, A., Mayda, S., 2004. Halitpaşa transpressive zone: implications for an Early Pliocene compressional phase in central western Anatolia, Turkey. *Turkish Journal of Earth Sciences*, **13**: 1–13.
- Kaymakçı, N., Langereis, C., Özkaptan, M., Özacar, A.A., Gülyüz, E., Uzel, B., Sözbilir, H., 2017. Fethiye-Burdur Fault Zone (SW Turkey): a myth? *Geophysical Research Abstracts*, **19**, EGU2017-5443-1.
- Keller, E.A., Pinter, N., 2002. *Active Tectonics: Earthquakes, Uplift, and Landscape*. Prentice Hall, New Jersey.
- Kirby, E., Whipple, K.X., 2012. Expression of active tectonics in erosional landscapes. *Journal of Structural Geology*, **44**: 54–75. <https://doi.org/10.1016/j.jsg.2012.07.009>
- Kissel, C., Poisson, A., 1987. Étude paléomagnétique des formations Cénozoïques des Bey Dagları (Taurides occidentales). *Comptes Rendue de l'Academie des Sciences de Paris*, **304**: 343–348.
- Kissel, C., Averbuch, O., Frizon de Lamotte, D., Monod, O., Allerton, S., 1993. First paleomagnetic evidence of a post-Eocene clockwise rotation of the western Taurus belt, east of the Isparta reentrant (southwestern Turkey). *Earth and Planetary Science Letters*, **117**: 1–14; [https://doi.org/10.1016/0012-821X\(93\)90113-N](https://doi.org/10.1016/0012-821X(93)90113-N)
- Koçyiğit, A., 1981. Evolution of Taurus Carbonate Platform in Isparta bend (western Taurus) (in Turkish with English summary). *Bulletin of the Geological Society of Turkey*, **24**: 15–23.

- Koçyiğit, A., 1983.** Tectonics of the Hoyran Lake (Isparta Bend) region (in Turkish with English summary). *Bulletin of the Geological Society of Turkey*, **26**: 1–10.
- Koçyiğit, A., Özacar, A.A., 2003.** Extensional neotectonic regime through the NE edge of the outer Isparta Angle, SW Turkey: new field and seismic data. *Turkish Journal of Earth Sciences*, **12**: 67–90.
- Koçyiğit, A., Yusufoglu, H., Bozkurt, E., 1999.** Evidence from the Gediz Graben for episodic two-stage extension in western Turkey. *Journal of the Geological Society*, **156**: 605–616; <https://doi.org/605-616>. [10.1144/gsjgs.156.3.0605](https://doi.org/10.1144/gsjgs.156.3.0605)
- Koçyiğit, A., Ünay, E., Saraç, G., 2000.** Episodic graben formation and extensional neotectonic regime in west central Anatolia and the Isparta Angle: a case study in the Akşehir-Afyon Graben, Turkey. *Geological Society Special Publications*, **173**: 405–421; <https://doi.org/10.1144/GSL.SP.2000.173.01.19>
- KOERI, 2023.** Recent Earthquakes in Turkey [online]. Website <http://www.koeri.boun.edu.tr/scripts/lasteq.asp> (accessed date: 20 January 2023)
- Kurt, H., Demirbağ, E., Kuşçu, İ., 1999.** Investigation of the submarine active tectonism in the Gulf of Gökova, southwest Anatolia–southeast Aegean Sea, by multi-channel seismic reflection data. *Tectonophysics*, **305**: 477–496; [https://doi.org/10.1016/s0040-1951\(99\)00037-2](https://doi.org/10.1016/s0040-1951(99)00037-2)
- Kürçer, A., Özdemir, E., Olgun, Ş., Özalp, S., Çan, T., Elmacı, H., 2021.** Active tectonic and paleoseismological characteristics of the Dinar Fault, SW Anatolia, Turkey. *Mediterranean Geoscience Reviews*, **3**: 219–251; <https://doi.org/10.1007/s42990-021-00052-x>
- Le Pichon, X., Angelier, J., 1979.** The Hellenic arc and trench system: a key to the neotectonic evolution of the eastern Mediterranean area. *Tectonophysics*, **60**: 1–42; [https://doi.org/10.1016/0040-1951\(79\)90131-8](https://doi.org/10.1016/0040-1951(79)90131-8)
- Le Pichon, X., Chamot-Rooke, N., Lallemand, S., 1995.** Geodetic determination of the kinematics of central Greece with respect to Europe: Implications for eastern Mediterranean tectonics. *Journal of Geophysical Research*, **100**: 12675–12690; <https://doi.org/10.1029/95JB00317>
- McClusky, S., Balassanian, S., Barka, A., Demir, C., Ergintav, S., Georgiev, I., Gürkan, O., Hamburger, M., Hurst, K., Kahle, H., Kastens, K., Kekelidze, G., King, R., Kotzev, V., Lenk, O., Mahmoud, S., Mishin, A., Nadariya, M., Ouzounis, A., Paradissis, D., Peter, Y., Prilepin, M., Reilinger, R., Sanli, I., Seeger, H., Tealeb, A., Toksöz, M.N., Veis, G., 2000.** Global Positioning System constraints on plate kinematics and dynamics in the eastern Mediterranean and Caucasus. *Journal of Geophysical Research*, **105**: 5695–5719; <http://dx.doi.org/10.1029/1999JB900351>
- McKenzie, D.P., 1978.** Active tectonics of the Alpine-Himalayan belt: the Aegean Sea and surrounding region. *Geophysical Journal of the Royal Astronomical Society*, **55**: 217–254; <https://doi.org/10.1111/j.1365-246X.1978.tb04759.x>
- Meulenkaamp, J.E., Wortel, W.J.R., Van Wamel, W.A., Spakman, W., Hoogerduyn Strating, E., 1988.** On the Hellenic subduction zone and geodynamic evolution of Crete in the late middle Miocene. *Tectonophysics*, **146**: 203–215; [https://doi.org/10.1016/0040-1951\(88\)90091-1](https://doi.org/10.1016/0040-1951(88)90091-1)
- Morris, A., Robertson, A.H.F., 1993.** Miocene remagnetisation of Mesozoic Antalya complex units in the Isparta Angle, SW Turkey. *Tectonophysics*, **220**: 243–266; [https://doi.org/10.1016/0040-1951\(93\)90234-B](https://doi.org/10.1016/0040-1951(93)90234-B)
- Ouimet, W.B., Whipple, K.X., Granger D.E., 2009.** Beyond threshold hillslopes: Channel adjustment to base-level fall in tectonically active mountain ranges. *Geology*, **37**: 579–582.
- Özalp, S., Elmacı, H., Kara, M., Güldoğan, Ç.U., Gürboğa, Ş., Duygu, L., 2017.** Paleoseismological data related to the earthquake activity of the Kumdanlı Fault, Isparta Angle, SW Anatolia. 70<sup>th</sup> Geological Congress of Turkey, 10–14 April 2017, Ankara, Abstracts: 596–597.
- Özalp, S., Emre, Ö., Şaroğlu, F., Özaksoy, V., Elmacı, H., Duman, T.Y., 2018.** Active fault segmentation of the Çivril Graben System and surface rupture of the 1 October 1995 Dinar earthquake (Mw 6.2), Southwestern Anatolia, Turkey. *Journal of Asian Earth Sciences*, **166**: 136–151; <https://doi.org/10.1016/j.jseaes.2018.07.037>
- Özener, H., Doğru, A., Acar, M., 2013.** Determination of the displacements along the Tuzla fault (Aegean region Turkey): preliminary results from GPS and precise leveling techniques. *Journal of Geodynamics*, **67**: 13–20; <https://doi.org/10.1016/j.jog.2012.06.001>
- Özgül, N., Bölükbaşı, S., Alkan, H., Korucu, M., 1991.** Kırdag-Barla Dağları-Davras Dağı Yöresinin Jeolojisi (Geology of Kırdag-Barla Dağları-Davras Dağı Area). General Directorate of Turkish Petroleum Corporation, Report No 314, Ankara (unpublished)
- Özkaymak, Ç., 2014.** Tectonic analysis of the Honaz fault (western Anatolia) using geomorphic indices and the regional implications. *Geodinamica Acta*, **27**: 110–129; <https://doi.org/10.1080/09853111.2014.957504>
- Özkaymak, Ç., Sözbilir, H., 2012.** Tectonic geomorphology of the Spiladağ high ranges, western Anatolia. *Geomorphology*, **173-174**: 128–140; <https://doi.org/10.1016/j.geomorph.2012.06.003>
- Özsayın, E., 2016.** Relative tectonic activity assessment of the Çameli Basin, Western Anatolia, using geomorphic indices. *Geodinamica Acta*, **28**: 241–253; <https://doi.org/10.1080/09853111.2015.1128180>
- Özsayın, E., Dirik, K., 2011.** The role of oroclinal bending in the structural evolution of the Central Anatolian Plateau: evidence from a regional changeover of shortening to extension. *Geologica Carpathica*, **62**: 345–359; <https://doi.org/10.2478/v10096-011-0026-7>
- Özsayın, E., Dirik, K., Ocakoğlu, F., Açıkalin, S., Sağlam Selçuk, A., 2023.** Relative tectonic activity assessment of the Bozdoğan and Karacasu grabens using geomorphic indices, Western Anatolia. *Geologica Acta*, **21**: 1–14; <https://doi.org/10.1344/GeologicaActa2023.21.1>
- Öztürk, E.M., Öztürk, Z., 1989.** Geology of the Balçıkhisar-Karaadilli (Afyon)-Dereköy (Isparta) and Surroundings (in Turkish). General Directorate of Mineral Research and Exploration, Archive no: 8946 (unpublished).
- Peacock, D.C.P., Knipe, R.J., Sanderson, D.J., 2000.** Glossary of normal faults. *Journal of Structural Geology*, **22**: 291–305; [https://doi.org/10.1016/S0191-8141\(00\)80102-9](https://doi.org/10.1016/S0191-8141(00)80102-9)
- Pérez-Peña, J.V., Azor, A., Azañón, J.M., Keller, E.A., 2010.** Active tectonics in the Sierra Nevada (Betic Cordillera, SE Spain): insights from geomorphic indexes and drainage pattern analysis. *Geomorphology*, **119**: 74–87; <https://doi.org/10.1016/j.geomorph.2010.02.020>
- Piper, J.D.A., Gürsoy, H., Tatar, O., İşseven, T., Koçyiğit, A., 2002.** Paleomagnetic evidence for the Gondwanian origin of the Taurides and rotation of the Isparta Angle, southern Turkey. *Geological Journal*, **37**: 317–336; <https://doi.org/10.1002/gj.920>
- Ramírez-Herrera, M.T., 1998.** Geomorphic assessment of active tectonics in the Acambay graben, Mexican Volcanic Belt. *Earth Surface Processes and Landforms*, **23**: 317–332; [https://doi.org/10.1002/\(SICI\)1096-9837\(199804\)23:4<317::AID-ESP845>3.3.CO;2-M](https://doi.org/10.1002/(SICI)1096-9837(199804)23:4<317::AID-ESP845>3.3.CO;2-M)
- Reilinger, R.E., McClusky, S.C., Oral, M.B., King, W., Toksöz, M.N., 1997.** Global Positioning System measurements of present-day crustal movements in the Arabian-Africa-Eurasia plate collision zone. *Journal of Geophysical Research*, **102**: 9983–9999; <https://doi.org/10.1029/96JB03736>
- Reilinger, R., McClusky, S., Paradissis, D., Ergintav, S., Vernant, P., 2010.** Geodetic constraints on the tectonic evolution of the Aegean region and strain accumulation along the Hellenic subduction zone. *Tectonophysics*, **488**: 22–30. <https://doi.org/10.1016/j.tecto.2009.05.027>
- Rockwell, T.K., Keller, E.A., Johnson, D.L., 1984.** Tectonic geomorphology of alluvial fans and mountain fronts near Ventura, California. In: *Tectonic Geomorphology* (ed. M. Morisawa): 183–207. Proceedings of the 15<sup>th</sup> Annual Geomorphology Symposium, Allen and Unwin Publishers, Boston, MA.

- Sağlam-Selçuk, A., 2016.** Evaluation of the relative tectonic activity in the eastern Lake Van basin, East Turkey. *Geomorphology*, **270**: 9–21; <https://doi.org/10.1016/j.geomorph.2016.07.009>
- Sağlam-Selçuk, A., Kul, A.Ö., 2021.** Long-term slip rate estimation for Erciș Fault in East Anatolian Compressive Tectonic Block from geologic and geomorphologic field evidence. *Geological Journal*, **56**: 5290–5310; <https://doi.org/10.1002/gj.4237>
- Scotti, V.N., Molin, P., Faccenna, C., Soligo, M., Casas-Sainz, A., 2014.** The influence of surface and tectonic processes on landscape evolution of the Iberian Chain (Spain): quantitative geomorphological analysis and geochronology. *Geomorphology*, **206**: 37–57; <https://doi.org/10.1016/j.geomorph.2013.09.017>
- Selby, M.J., 1980.** A rock strength classification for geomorphic purposes: With tests from Antarctica and New Zealand. *Zeitschrift für Geomorphologie*, **24**: 31–51; <https://doi.org/10.1127/zfg/24/1984/31>
- Seyitoğlu, G., Scott, B., 1991.** Late Cenozoic crustal extension and basin formation in west Turkey. *Geological Magazine*, **128**: 155–166; <https://doi.org/10.1017/S0016756800018343>
- Seyitoğlu, G., Scott, B., 1992.** The age of the Büyük Menderes Graben (western Turkey) and its tectonic implications. *Geological Magazine*, **129**: 239–242; <https://doi.org/10.1017/S001675680000830X>
- Silva, P.G., Goy, J.L., Zazo, C., Bardají, T., 2003.** Fault-generated mountain fronts in southeast Spain: Geomorphologic assessment of tectonic and seismic activity. *Geomorphology*, **50**: 203–225; [https://doi.org/10.1016/S0169-555X\(02\)00215-5](https://doi.org/10.1016/S0169-555X(02)00215-5)
- Snyder, N.P., Whipple, K.X., Tucker, G.E., Merritts, D.J., 2003.** Channel response to tectonic forcing: field analysis of stream morphology and hydrology in the Mendocino triple junction region, northern California. *Geomorphology*, **53**: 97–127.
- Sözbilir, H., 2001.** Extensional tectonics and the geometry of related macroscopic structures: Field evidence from the Gediz Detachment, Western Turkey. *Turkish Journal of Earth Sciences*, **10**: 51–67.
- Sözbilir, H., 2002.** Geometry and origin of folding in the Neogene sediments of the Gediz Graben, western Anatolia, Turkey. *Geodinamica Acta*, **15**: 277–288.
- Şaroğlu, F., Emre, Ö., Boray, A., 1987.** Active Faults of Turkey and Their Seismicity (in Turkish). General Directorate of Mineral Research and Exploration, Archive No: 8174, 394p., Ankara, (unpublished).
- Şaroğlu, F., Emre, Ö., Kuşçu, İ., 1992.** Active Fault Map of Turkey (in Turkish). General Directorate of Mineral Research and Exploration, Ankara.
- Şenel, M., Dalkılıç, H., Gedik, İ., Serdaroğlu, M., Gözler, M.Z., 1981.** Geology of the southeastern Teke Taurus (in Turkish with English summary). *Bulletin of General Directorate of Mineral Research and Exploration*, **95-96**: 13–43.
- Şengör, A.M.C., 1979.** The North Anatolian Transform Fault: its age, offset and tectonic significance. *Journal of the Geological Society*, **136**: 269–282 <https://doi.org/10.1144/gsjgs.136.3.0269>
- Şengör, A.M.C., Yılmaz, Y., 1981.** Tethyan evolution of Turkey: a plate tectonic approach. *Tectonophysics*, **75**: 181–241; [https://doi.org/10.1016/0040-1951\(81\)90275-4](https://doi.org/10.1016/0040-1951(81)90275-4)
- Şengör, A.M.C., Yılmaz, Y., Sungurlu, O., 1984.** Tectonics of the Mediterranean Cimmerides: nature and evolution of the western termination of Palaeo-Tethys. *Geological Society Special Publications*, **17**: 117–152; <https://doi.org/10.1144/GSL.SP.1984.017.01.04>
- Şengör, A.M.C., Görür, N., Şaroğlu, F., 1985.** Strike-slip faulting and related basin formation in zones of tectonic escape: Turkey as a case study. *SEPM Special Publication*, **37**: 227–264.
- Taymaz, T., 1993.** The source parameters of the Çubukdağ (W. Turkey) earthquake of October 11. *Geophysical Journal International*, **113**: 260–267; <https://doi.org/10.1111/j.1365-246X.1993.tb02545.x>
- Taymaz, T., Price, S., 1992.** The 1971 May 12 Burdur earthquake sequence, SW Turkey: a synthesis of seismological and geological observations. *Geophysical Journal International*, **108**: 589–603; <https://doi.org/10.1111/j.1365-246X.1992.tb04638.x>
- Umut, M., 2009.** 1/100,000 scale Geological Maps of Turkey. General Directorate of Mineral Research and Exploration, Afyon L-26 Sheet (No: 119).
- Uysal, S., Dumont, J.F., Poisson, A., 1980.** Western Taurus plateforms (in Turkish with English summary). General Directorate of Mineral Research and Exploration, Archive No: 80 (unpublished).
- Valkanou, K., Karymbalis, E., Papanastassiou, D., Soldati, M., Chalkias, C., Gaki-Papanastassiou, K., 2020.** Metamorphometric analysis for the assessment of relative tectonic activity in Evia Island, Greece. *Geosciences*, **10**: 1–15; <https://doi.org/10.3390/geosciences10070264>
- Van Hinsbergen, D.J.J., Torsvik, T.H., Schmid, S.M., Matenco, L.C., Maffione, M., Vissers, R.L., Gürer, D., Spakman, W., 2020.** Orogenic architecture of the Mediterranean region and kinematic reconstruction of its tectonic evolution since the Triassic. *Gondwana Research*, **81**: 79–229; <https://doi.org/10.1016/j.gr.2019.07.009>
- Waldron, J.W.F., 1982.** Stratigraphy and sedimentary evolution of the NE Antalya Complex: Isparta Province, Turkey (in Turkish with English summary). *Bulletin of General Directorate of Mineral Research and Exploration*, **97-98**: 1–20.
- Westaway, R., 2003.** Kinematics of the Middle East and the Eastern Mediterranean updated. *Turkish Journal of Earth Sciences*, **12**: 5–46.
- Westaway, R., Pringle, M., Yurtmen, S., Demir, T., Bridgland, D., Rowbotham, G., Maddy, D., 2003.** Pliocene and Quaternary surface uplift of western Turkey revealed by long-term river terrace sequences. *Current Science*, **84**: 1090–1101.
- Whipple, K.X., DiBiase, R.A., Crosby, B.T., 2013.** Bedrocks rivers. In: *Treatise on Geomorphology* (ed. J.F. Shroder): 550–573. Elsevier, Poland.
- Whittaker, A.C., 2012.** How do landscapes record tectonics and climate? *Lithosphere*, **4**: 160–164.
- Wobus, C., Whipple, K.X., Kirby, E., Synder, N., Johnson, J., Spyropoulou, K., Crosby, B., Sheehan, D., 2006.** Tectonics from topography: procedures, promise, and pitfalls. *GSA Special Papers*, **398**: 5–74; [https://doi.org/10.1130/2006.2398\(04\)](https://doi.org/10.1130/2006.2398(04))
- Yağmurlu, F., 1991.** Stratigraphy and depositional environments of Yalvaç-Yarıkkaya Neogene basin, SW-Anatolia (in Turkish with English summary). *Bulletin of General Directorate of Mineral Research and Exploration*, **112**: 1–12.
- Yıldırım, C., 2014.** Relative tectonic activity assessment of the Tuz Gölü Fault Zone Central Anatolia, Turkey. *Tectonophysics*, **630**: 183–192; <https://doi.org/10.1016/j.tecto.2014.05.023>
- Yılmaz, Y., Genç, S.C., Gürer, F., Bozcu, M., Yılmaz, K., Karacık, Z., Altunkaynak, Ş., Elmas, A., 2000.** When did the western Anatolian grabens begin to develop? *Geological Society Special Publications*, **173**: 353–384; <https://doi.org/10.1144/GSL.SP.2000.173.01.17>
- Zabci, C., 2020.** Morphometric characteristics of the Malatya Fault (in Turkish with English summary). *Türk Coğrafya Dergisi*, **75**: 107–118; <https://doi.org/10.17211/tcd.818850>